MINISTRY OF EDUCATION AND SCIENCE OF THE REPUBLIC KAZAKHSTAN
Non-commercial joint-stock company
«ALMATY UNIVERSITY OF POWERENGINEERING AND TELECOMMUNICATIONS»»
Institute of space engineering and telecommunications

«Approved for protection»
Head of the Institute of space engineering and telecommunications
____
Chigambayev T.O.
«___»__________2020

DIPLOMA PROJECT

On the topic: «Dynamic modeling and control off flexible manipulators»
Specialty «5B071600 – Instrumentation engineering»
Performed __________st. gr. PSa-16-4 Sultanmurat D.N.

Scientific adviser __________________Zhauyt A., ass. Prof.

Consultants::
on the economic side:
Tuzelbayev B.I., c.t.s, associate professor
________________ «____»_____________20____г.

on the safety of life:
Begimbetova A.S., senior lecturer
________________ «____»_____________20____г.

Normcontrol: Fazylova A.R., teacher

_______________ «____»______________20___г.

Reviewer: ___________________

______________ «____»______________20___г.
(sign)

Almaty 2020

MINISTRY OF EDUCATION AND SCIENCE OF THE REPUBLIC KAZAKHSTAN

Non-commercial joint-stock company

«ALMATY UNIVERSITY OF POWERENGINEERING AND TELECOMMUNICATIONS»»

Institute of space engineering and telecommunications.

Specialty «5B071600 – Instrumentation engineering»

Department: «Electronics and robotics»

TASK

for the completion of the diploma project

Student Sultanmurat D.N.

Topic: «Development of a flowmeter to control water level» approved by order of the rector № ___ from _ _ _ September 2019

Deadline for completion of completed work «__» _____ 2020

Source data for the project (required parameters of design results) and source data:

1) achieving desired endeffector trajectory tracking

2) suppressing vibrations of the endeffector

A list of issues to be developed in the diploma project or a summary of the diploma project::

1. Dynamic modeling
2. Control of flexible manipulators
3. Experimental Results
4. Characteristics of the simulink program
5. Analysis of working conditions in the room with personal computers
6. Feasibility study of the project

List of graphic material (with exact indication of mandatory drawings): this work contains 46 figures and 17 tables.

Recommended main references::

1. Albu-Schaffer, O. Eiberger, M. Grebenstein, S. Haddadin, C. Ott, T.

2. Wimbock, S. Wolf, and G. Hirzinger. Soft robotics: From torque feedback controlled lightweight robots to intrinsically compliant systems. *IEEE Robotics and Automation Mag.*, 15(3):20–30, 2008.
3. A. Daryabor, A.H. Abolmasoumi, and H. Momeni. . Robust pole placement control of flexible manipulator arm via lmis. *41st Southeastern Symposium on System Theory*, pages 274–279, 2009.

Project consultants with an indication of the work sections related to them

Section	Consultant	Deadlines	Sign
Dynamic modeling	Zhauyt A.		
Control of flexible manipulators	Zhauyt A.		
Analysis of flexible manipulators	Zhauyt A.		
Experimental Results	Zhauyt A.		
Economic part	Tuzelbayev B.I.		
Life safety	Begimbetova A.S.		

SCHEDULE

preparation of the diploma project

№	Name of sections, list of issues being developed	Deadlines for submission to the Scientific adviser	Note
1	2	3	4
1	Dynamic modeling		
2	Control of flexible manipulators		
3	Analysis of flexible manipulators		
4	Experimental Results		
5	Economic part		
6	Life safety		

Date the task was issued «___» __________ 2020

Head of department ________________ Chigambayev T.O.

Scientific adviser __________ Zhauyt A.

The task was accepted by the student _____________ Sultanmurat D.N.

(sign)

Андатпа

Дипломдық жоба динамикалық модельдеудің жүйелі тәсілін анықтауға және дамытуға арналған, ол икемділікті дәл қамтуы мүмкін және кеңістіктік икемді манипуляторларға қажетті траекторияны бақылау үшін модельді басқаруды әзірлеуге арналған. Динамикалық модельдеу және икемді манипуляторларды басқару жағдайлары талқыланады. Содан кейін зерттеу жұмысының мақсаты ұсынылады.

Аннотация

Дипломный проект посвящен определению и разработке системного подхода к динамическому моделированию, который может точно включать гибкость и разработку управления на основе модели для пространственных гибких манипуляторов для достижения желаемого отслеживания траектории. Обсуждается современное состояние динамического моделирования и управления гибкими манипуляторами. Цель исследовательской работы представлена.

Summary

The diploma project is dedicated to identify and develop a systematic approach for the dynamic modeling that can accurately include the flexibility and to develop model based control for spatial flexible manipulators to achieve desired trajectory tracking. The state of the art on the dynamic modeling and control of flexible manipulators is discussed. Then, the objective of the research work is presented.

Contents

Introduction

Robot manipulators are designed to increase the productivity and to help humans in tedious and hazardous work environment. The manipulator arms are made of heavy and stiff materials to achieve high precision on endeffector motion. However, the heavy manipulator arms are required to have bulky actuators for robot manipulation in workspace. In addition, the heavy manipulators have higher mass, consume more power and have limited operation speed with respect to operating payload. In order to built power efficient robot manipulators and to increase the operation speed, the focus is switched towards development of light weight manipulators [1].

The applications of lightweight manipulators can be found in space, construction, and medical field. In space applications, the space shuttle is equipped with a long reach manipulator to assist the astronauts in extra vehicular activities [2]. The Shuttle Remote Manipulation System (RMS), CANADARM shown in figure (1.1) is a 15.3 m long, 38 cm in diameter, and weighs 408 kg. It has six joints similar to that of human arm. The Shuttle RMS can handle payloads with masses up to 29,500 kg.

In construction applications, the truck mounted concrete boom structures shown in figure (1.2) is used to transport the concrete. These manipulators can have vertical movement up to 31.2 m, and horizontal movement up to 26.5 m.

Another attractive feature of light weight manipulators is safe to work along with human coworker and easy transportability. With these advantages, the use of light weight manipulators is emerging in the field of automotive, medical, and various general purpose industrial applications. The KUKA and DLR together developed such a light weight manipulator that, weighting 13.5 Kg, can handle 15 Kg load.

The benefits of light weight manipulators come at the cost of flexibility in joints, links or both. The Shuttle Remote Manipulation System (RMS), CANADARM shown in figure 1.1.

Figure 1.1 - Space shuttle remote manipulation system

For instance, KUKA DLR lightweight manipulator showed in figure 1.3 is treated as flexible joint manipulator due to the harmonic drive transmission, differential gear drive and frictional effect [3] [2]. The shuttle RMS [7] and concrete boom structure [6] have a long slender links made of lightweight materials treated as a flexible link manipulator. The flexible links can lead to vibrations on the end-effector and complex dynamic behavior to the whole system.

The control of light weight manipulators is complex based on the nature of flexibility in the system, i.e. flexible joints, flexible links or flexible joints and links. Among them, the most difficult task is to control the flexible link manipulators because of link flexibility, under actuation and non-minimal phase nature. Under actuation is due to finite number of actuators to control infinite degrees of freedom that arise due to link flexibility [5]. Non-minimum phase nature occurs because of non-collocation of actuators and sensors [7].

Despite of various advantages, the flexible link manipulators have less the progress at the industrial level. There is a need to bring the advantages of flexible link manipulators to more general industrial applications by eliminating the difficulties surrounded to it such as modeling link flexibility, under actuation and non-minimum phase nature in control design. The dynamic modeling that includes the link or joint flexibility is considered as an important step in model based control design and to achieve better performance. The following research work is dedicated to identify and develop a systematic approach for the dynamic modeling and model based control of spatial flexible manipulators.

1 Introduction

1.1 State of the art

The state of the art on dynamic modeling and control of flexible manipulators are discussed in this section. At first the various dynamic formulations and techniques for the modeling of flexible manipulators are presented. Then, the control techniques to achieve desired trajectory tracking and vibration suppression are presented. The truck mounted concrete boom structures shown in figure 1.2.

Figure 1.2 - Truck mounted concrete boom pump

KUKA DLR lightweight manipulator showed in figure 1.3.

Figure 1.3 - Kuka DLR Light weight robot

1.1.1 Dynamic modeling of flexible manipulators

Dynamic modeling is an important step in the control design process. The performance of the controller mainly depends on the accuracy of the dynamic models that are used in control design.

The dynamics of the robot manipulators can be derived using various methods such as Newton-Euler, principle of virtual work, Lagrangian-Euler, Gibbs-Appell, Hamilton principle. Many algorithms were developed based on these methods to define equations of motion.

The inclusion of the dynamics due to flexibility makes the robot manipulator a highly nonlinear model. It also establishes strong coupling between gross rigid body motion and elastic deformations of links or joints. The techniques to model flexibility in manipulator dynamics are presented below.

Flexible Joint Manipulators

Flexible joint manipulators are assumed to have rigid links and flexible joints. In [8] the joint flexibility was modeled as a linear spring and showed that as the stiffness goes to infinity the model behaves like a rigid manipulator.

In [5] the dynamic model of two revolute joint robot with flexible joint is derived. The flexible joint have servo stiffness and damping modeled along with stiffness and damping of drive system. A series of simple torsional spring is used to model servo stiffness and drive stiffness. The resulting torque stiffness equation at joints along with equations of motion of rigid links is a highly coupled nonlinear ordinary differential equations. From the numerical investigation, it is concluded that the servo damping plays an important role in dynamic response of the system.

A generic dynamic model was developed in [1] for an industrial KUKA IR 761 robot manipulator which includes joint elasticity due to electric drives. In [9], the dynamics of a n-link flexible manipulator was modeled with revolute flexible joints described as a linear torsional spring with known stiffness.

The DLR medical robot in [4] is a redundant robot with 4 flexible joints. It considers the elasticity of joint due to harmonic drive and differential gear transmission. The elastic joint was modeled as a linear torsional spring. The resulting dynamic model has a strong coupling between the flexible joint and link motion.

Flexible Link Manipulator

Flexible link manipulators are assumed to have rigid joints and flexible links. The links are considered to have low stiffness because of lightweight materials. The dynamics of link flexibility can be modeled using Euler-Bernoulli beam equation or Timoshenko beam equation.

The dynamics of beam deformations can be described using partial differential equation. With the inclusion of dynamics due to link flexibility, the dynamic model takes the form of coupled nonlinear ordinary and partial differential equation. The flexible link manipulator system has distributed dynamic parameters which are characterized by infinite number of degrees of freedom. The exact solution of such systems is not feasible. To simplify the modeling process, the continuous systems can be discretized by using assumed mode method (AMM), finite element method (FEM), finite difference method (FDM) and Lumped parameter method (LPM).

Assumed Mode Method

In AMM, the flexibility of link is truncated to obtain finite number of modes that can accurately represent the dynamic parameters of the flexible link. This method assumes the deflection of link is small and expresses the deflection as summation of finite number modes. Each mode is defined as product of two functions, first as a function of distance along manipulator length and other function as generalized coordinates depending on time.

In [3], the dynamic model was developed using recursive Lagrangian approach via transformation matrix and modeled the link flexibility using AMM. The transformation matrix is a 4x4 matrix that includes the joint flexibility. This method is an extension to classical rigid body transformation matrix. The advantage of this approach is that it represents both joint and link deflection motion in the form of transformation matrix and can be easily used in algorithm implementation.

A closed form dynamic modeling approach for a planar multi-link manipulators were presented in [4]. A Lagrangian approach and AMM was used to model the dynamics of planar multi-link flexible manipulator.

In [2], a linearized dynamic model for a multi-link planar flexible manipulator was derived using Euler-Lagrangian formulation and AMM. The dynamic model is linearized around rigid body motion to decouple the rigid and elastic deformation of manipulator.

The truncated modes of flexible link to approximate the dynamic behavior of system are not the same when the manipulator has a payload mass on the endeffector. The effect of endeffector payload mass on the modes of flexible link was studied in [2] [5]. A two link planar flexible manipulator was considered to study the dynamics of system with additional payload mass on endeffector. In those studies, a closed form dynamic equation using Euler-Lagrangian formulation and AMM was derived to show the effect of payload on dynamic behavior of the system.

There were number of research studies on AMM because of the simplicity in dynamic formulation. However, the main drawback of this method is that it is difficult to find modes for non-regular cross-sections. And the choice of boundary conditions for multilink manipulator is not unique. The possible boundary conditions reported in the literature are clamped, pinned-pinned, free-free boundary conditions. In [2], it was reported that if the beam to hub inertia ratio is small, the clamped boundary condition yields better results than pinned boundary conditions.

Finite Element Method

Using Finite element method, the drawbacks of AMM such as defining boundary conditions and irregular geometry can be accounted in a straightforward way. In this method, the continuous flexible links are divided in number of small elements. The displacements at any point on the link are expressed in terms of nodal displacements and polynomial interpolation function defined in element. The dynamics of each finite element is derived first then the elements are assembled based on element connectivity to obtain dynamics of the whole system.

The comparison between two discretization techniques such as AMM and FEM was studied in [4] to efficiently define link flexibility in manipulator dynamics. Lagrangian equation was used to derive closed form dynamic equations of motions. The numerical results were presented for a flexible spherical (RRP) manipulator and stated that FEM overestimates the structural stiffness but it takes fewer operations to compute inertia matrix.

A general purpose computer program SPACAR for numerical simulations of flexible mechanism and manipulators was developed in [3]. SPACAR used a finite element based Lagrangian formulation to define dynamics of the system. The program was incorporated with virtual power type approach, to automatically eliminate the nonworking constraints forces and reactions. This approach leads the Lagrangian formulation into a minimal set of ordinary differential equations.

In [7] the numerical and experimental investigation on dynamic modeling of flexible manipulators was done. A planar constrained model was considered for dynamic model verification. The dynamic model was developed using Lagrangian approach and finite element method. The experimental validation was carried out on a single link flexible manipulator and compared with numerical finite element model in both frequency and time domain. The FEM model showed closer agreement with the experimental results.

A redundant Lagrangian FEM formulation for the dynamic modeling of flexible links and joints was presented in [7]. The elastic deformation on each link is assumed due to bending and torsion. The deformation of each link is expressed in tangential local floating frame. The constrained equations due to connectivity of each link are added to equations of motion by using Lagrangian multiplier. Other works on dynamic modeling of spatial flexible manipulator based on Lagrangian formulation and FEM were addressed in [7] [4].

The advantage of FEM method is that it can consider complex geometric shapes and have no difficulties in defining the boundary conditions that exist in AMM. Other important thing is that it can make use of existing and well defined FEM algorithms for dynamic modeling of flexible manipulators to accurately define rigid and flexible dynamics.

Finite Difference Method

Finite difference method is also used to approximate the dynamic characteristics of flexible manipulators. This method discretizes the system into several segments and develops a linear relation for deflection of the end of each segments using finite difference approximation.

An algorithm was proposed for a real time simulation of flexible manipulator using FDM in [5]. The performance of the algorithm was tested on a single link flexible incorporating hub inertia and payload.

In [6] the study on FEM and FDM was done to investigate the dynamic characteristics of the flexible manipulator system based on the accuracy, computational efficiency and computational requirement. Both methods were compared on a single link flexible manipulator and the results demonstrated that FEM representation was more accurate and more efficient performance can be achieved compared to FDM.

Lumped Parameter Method

Lumped Parameter method is a simple method to model the dynamics of flexible link. This method basically defines the continuous flexible link as lumped masses and massless springs. There are two approaches to define the characteristics of concentrated mass and springs. One of them is a numerical approach that uses finite element method or Holzer method [15]. The other one is an experimental approach that uses a series of experiments to define parameters of a flexible link.

In [8] the finite element method associated with model analysis was used to model distributed system into lumped parameter model. The lumped parameter model was defined as a cascade system of concentrated point masses and weightless linear and angular spring.

In Holzer method [2] the flexible link was partitioned in to small divisions. The total mass of each division is treated as two equal concentrated masses at the ends of division. The lumped mass on the division points is connected by an elastomer without mass. The lumped mass is also called as station and elastomer between lumped mass is called field.

In [9] the lumped parameter model of flexible link was defined using equivalent representation of virtual rigid link and passive joints such as springs and dampers. The parameters of virtual rigid link and passive joints were identified by using measured data of real flexible link.

The advantage of lumped parameter method is that it does not involve complex mode shape functions compared to finite element method and assumed mode method. However, it cannot be used if the flexible link manipulator has complex geometric shapes.

1.1.2 Control of flexible manipulators

The primary objective of control for a flexible link manipulator is to compute input torque necessary to drive the system in a desired trajectory and minimizing the oscillation of the tip. The dynamic model of flexible manipulator is a nonlinear and coupled differential equation. As stated in previous section, strong coupling exists between the rigid body motion and the elastic modes. In control design, there should be a compromise between rigid and elastic modes to achieve desired performance.

Many model based controllers were developed for flexible manipulators to achieve desired trajectory tracking and vibration suppression. These are designed based on the control schemes available for linear and nonlinear dynamic systems. Some of them used a linearized dynamic model to simplify control design process. Moreover, the linear control techniques to analyze system stability and robustness properties are very well established.

The following nonlinear control techniques are widely used to design the controller for flexible manipulator, i.e open loop method, feedback linearization method, singular perturbation method, stable inversion method, Robust control, Adaptive control, sliding mode technique, pole placement method, output redefinition, lead-lag control, iterative learning method, and intelligent control methods such as Fuzzy Logic control, Neural Network control.

Open loop method

In open loop control, the input signal is computed based on reference trajectory and vibrations are controlled by modifying the input signal considering the physical and vibrational properties of flexible link manipulators. The open loop control methods developed for flexible link manipulators are command shaping method and computed torque method based on model inversion.

A command shaping method for a single link flexible manipulator was proposed in [7]. This method computes the input signal required for a rest to rest motion in a finite time and reduces the vibration of flexible link. The advantage of this method is that it computes the input signal to suppress vibrations without measurement data by solving a set of linear equation.

In [1] a feedforward control based on input shaping technique was proposed to suppress vibrations. In the experiments, an unshaped bang-bang torque was used to determine the dynamic parameters of the system. The parameters are then used in input shaping technique to suppress vibrations.

In computed torque method, the input torque is computed using model inversion based of the desired output trajectory. In [6] a feedforward control was developed based on inverse dynamic model. The dynamic model was derived in the form of differential algebraic equations. In [1], an energy saving open loop control scheme was proposed for a single link flexible manipulator to perform point to point motion in a fixed time. For a given tip trajectory, the joint angle was computed using Artificial Neural Network, and vector evaluated particle swarm optimization was used as a learning algorithm. The vibration suppression was realized along the joint trajectory using minimum driving energy consumption. This method has an advantage of energy saving because the residual vibrations are suppressed without measuring vibrations.

The open loop control methods are simple and require less measurement but they are very sensitive to the model inaccuracy, system parameter variation, and uncertainty in the implementation of desired trajectory. To overcome these issues, a feedback is necessary to monitor the system behavior to improve the performance of the controller and ensure stability of the system.

Feedback linearization Method

The first published and known work on feedback control of flexible manipulator was presented in [4]. The theoretical studies of PD feedback control of two-link two joint robot manipulator was presented. The joint position and velocity errors are used in feedback loop with constant gains. The gains were calculated based on vibrational properties to damp out the vibrations. The stability of the closed loop control was analyzed using root-locus method.

In [4] studied extensively on control of flexible arms and influence of unmodeled dynamics in the system controllability and performance which is widely known as spillover. After successful studies on different control challenges, there was a need to develop and test these techniques on real platform. The first known flexible arm of single link was developed at Aerospace robotics lab in Stanford University. In [3] experimental studies on precise positioning of flexible arm by sensing the tip and arm joint position are carried out. In this work, the concepts of non-collocated system robot and non-minimum phase nature were addressed.

In [9] a model based controller was proposed using approximate inverse dynamics and passive feedback control for a six degrees of freedom manipulator with flexible links. In this approach, the non-minimum phase nature of the system is solved by introducing μ-tip rate which is output of the system and passive to input torque. The actual tip position is approximated by μ-tip position using joint angles and elastic coordinates by a parameter μ. The global asymptotic stability was proved using Lyapuonv function for a PD feedback control. The advantage of this approach is that it does not require measurement of elastic coordinates; the controller provides stable tracking by just using joint angles and rates plus endeffector position and rates.

The collocated and noncollocated PD control for a single link manipulator was proposed in [8]. Minimum phase system is achieved by exact transfer function which has joint torque as input and joint angle plus weighted value of tip deflection as an output. The non-minimum phase nature occurs when the tip position is considered as an output. In this approach, the output of the link i.e. tip position is defined as joint angle plus weighted value of tip deflection. The conditions for weighted value of tip is defined using infinite product expansion, root locus method such that the transfer function does not have any open right half plane zeros.

Singular Perturbation Method

A Singular perturbation approach can be applied to control rigid body motion and stabilize vibration along the trajectory. A well know work of trajectory control using singular perturbation approach is in [6]. Using this approach, the system dynamics are divided into slow and fast dynamics and a two stage controller was developed to tackle system vibrations and trajectory tracking. Slow dynamics are mainly to control the rigid body motion along the predefined trajectory along joint space. Fast dynamics are responsible for stability of vibrations along the joint trajectory. In this approach, the spill over problem in the fast dynamics is bounded by a perturbation parameter. Later on, this approach is applied to design many controllers. Fast dynamic control and slow dynamics control are controlled separately and many improvements are made on each control to achieve desired performance.

A robust-optimal controller was proposed in [7] for a single link flexible manipulator using singular perturbation approach. Slow dynamics (rigid modes) are controlled using sliding mode method and optimal LQR is designed to stabilize the fast dynamics (flexible modes). Angular position error is used to control rigid body dynamics, tip deflections are measured using strain gauge. The proposed controller tested on a real platform and the results showed good stability along trajectory.

A composite controller was developed in [6] for a three link spatial flexible manipulator using singular perturbation method. The composite controller is based on Cartesian based PI control for endeffector trajectory tracking and pole placement feedback control to damp the vibrations along trajectory. The advantage of this method is it does not require derivative of the endeffector position, and derivatives of strain gauge in the feedback loop. The proposed controller was tested on a real platform FLEBOT II.

Stable Inversion Method

Stable Inversion Method is another method widely used to design trajectory control of flexible link manipulators. In this method, the dynamic model is inverted in the form of Input-Output terms. In dynamic model inversion, the system has a non-minimum phase nature when the endeffector is considered as output. There are several approaches to make the model inversion stable in control design for trajectory tracking.

In [9] a joint based inversion approach was used to overcome the non-minimum phase nature. In this case, the output of the system is considered as joint coordinates. In this form, the model inversion has acceleration as an input and torque as an output. To compute the torque corresponding to the desired endeffector trajectory with minimum vibrations, both joint and elastic states are required. The elastic states for the reference joint based trajectory should be computed first by solving the internal dynamics offline. In addition to computed torque for the desired reference trajectory, the system has a PD feedback loop for a joint trajectory tracking to make control robust. The proposed stable inversion control is robust at joint space and the vibrations are suppressed by solving the internal dynamic off-line. However, it does not consider the endeffector in the control loop, so the stability of tip vibrations is not guaranteed always.

Later on, the output of the system i.e. tip position is defined as joint coordinates plus weighted value of tip deflection [2] for accurate endeffector trajectory tracking. As usual, the model inversion has unobservable internal dynamics i.e. elastic states for the reference trajectory. Three methods were proposed to solve internal dynamics i.e. approximate non-linear regulation, Iterative inversion in frequency domain, Iterative learning in time domain [8] [13] [11]. Experimental results were presented on a two link flexible manipulator FLEXARM to show the robustness of the proposed stable inversion method. The disadvantage of these approaches is that the internal dynamics should be solved first off-line.

The stable Inversion method in time domain and frequency domain was used in [2] [3]. In [3], a model inversion method was proposed for endeffector tracking of flexible manipulator. It takes end point acceleration as input and computes the torque in frequency domain. The proposed model inversion is non-causal, because the output, i.e. torque, must begin before the input, i.e. where the end point acceleration begins. This approach showed good results for end point trajectory tracking but have the disadvantage of excessive computation burden due to dynamic model; input trajectory should be transformed from time domain to frequency domain and output should be transformed back to time domain. Later on, a convolution integration method [4] was used to reduce this computational burden.

In [1], dynamic model inversion was proposed in time domain to reduce the computation effort. The inverse dynamic model is treated as causal part and anti-casual part to compute bounded torque for endpoint trajectory. This model can produce the accurate endpoint trajectory but shows some position error due to present of friction at joint. A simple PD feedback control loop is introduced to compensate the frictional effects.

Recently, in [2] a stable inversion method for two link flexible manipulator is proposed. The dynamic system is converted into the input-output form. The output of the system is considered as joint angles plus weighted value of the tip deflection. To compute the bounded torque required for given reference trajectory, bounded elastic states are computed first by solving internal dynamics as a two sided boundary problem using MATLAB bvp5c solver. In addition, a design optimization was proposed for choosing weights of tip deflection. Some of the other works on stable inversion method for flexible manipulators can be referred in [8], [5], [1], [6], and [4].

The stable inversion method proposed in the literature for a flexible link manipulator assumes the dynamic model is accurate such that zero and poles of the system can be located accurately. It does not consider the model uncertainty; any model parameter such as mass of the link, stiffness, and unknown payload mass on the endeffector can alter the location of poles and zeros of the system. In this case, stability of the system is no longer assured using stable inversion method.

Robust control

The robust controllers were proposed for accurate trajectory tracking of flexible manipulators in the presence of unknown payload, and parameter uncertainty such as stiffness and joint friction. In [5], a robust control design was proposed for a single link flexible manipulators. The model uncertainty was considered due to stiffness, damping, and payload mass. Uncertainty of payload in left-hand side of inertia matrix and uncertainty parameters included in right-hand side stiffness and damping are treated with polytopic and descaling techniques respectively. Then robust controller design problem is solved using linear matrix inequalitys (LMI).

In [3], a robust pole placement control was proposed using dynamic output feedback. The robustness of the controller is analyzed using LMI techniques. In [65] addressed the unstable closed loop response due to over-estimation of natural frequency from dynamic model derived from finite element method. A robustness of the controller is analyzed using second method Lyapunov function for a bounded model uncertainty. The proposed robust controller is a two stage controller, first stage controller is responsible for stable joint trajectory tracking and second stage controller is to suppress vibrations of the tip.

In [9] and [1] a robust controllers for flexible manipulators is proposed and the robustness of the system using μ-synthesis is analyzed. In [9] designed a collocated and noncollocated controller, and considered the model uncertainties are due to unmolded high frequency dynamics, error in natural frequencies, damping levels, actuators and sensors.

Robust controller are designed, analyzed and proved to be stable in the presence of bounded model uncertainty. When model uncertainties are large and cannot estimate the bounds of uncertainty, then robust controllers may not guarantee the stability. To overcome these difficulties and to make controller stable in unknown parameter uncertainty, adaptive controllers were proposed for flexible manipulators.

Adaptive control

Adaptive control for flexible link manipulators is designed mainly for accurate trajectory tracking and stabilizes tip vibrations for large unknown payload mass. The nonlinear dynamic system of flexible manipulator can be expressed in the fixed parameter form, which is the product of regression term and an unknown constant parameter.

An adaptive controller was proposed in [8] for a flexible link manipulator carrying payload much greater than manipulator mass. The input-output mapping of flexible manipulator was defined using μ-tip rate similar to [9] and a passive approach to solve non-minimum phase nature was applied. The passive nature of the output and fixed parameter form of system dynamics allows us to easily extend the rigid body adaptive controllers to flexible arms. The controller has feedforward term which is adaptive form and strictly passive PD feedback law. The adaptive controller ensures global stable tracking of cartesian endeffector coordinates with the help of only tip position and rate error.

The extended version of adaptive controller was proposed in [5]; a joint space feedforward term is derived for multilink case where task space dynamics is non-trivial. The proposed task space adaptive control and joint space adaptive control was experimentally verified on a three link planar manipulator that has one rigid link and two flexible links.

In [6] an adaptive variable structure was proposed for flexible link manipulators. The dynamics of flexible link manipulator was converted from the flexible mode dependent dynamics to strain dependent one, to reduce online computation burden on feedback signal of the flexible modes. The nonlinear dynamics of the flexible manipulator was expressed as a linear-in-parameter form for the feedforward term. The stability of the systems was analyzed using Lyapunov function. The advantage of this approach is that it has less computational effort and just uses strain measurement in the feedback loop instead of complete elastic mode information. But, the adaptive variable structure scheme comes with chattering effect along the trajectory. To overcome this effect a saturation type adaptive law was proposed.

A nonlinear controller law both in non-adaptive and adaptive version was compared numerically and experimentally on a two link flexible manipulator [7]. The controller ensures accurate joint space trajectory tracking using joint position and velocity measurement and vibration suppression using strain measurement. The stability of the controller was analyzed using Lyapunov analysis. To avoid spillover problem, a second order analog filter in strain gauge amplifier and first order analog filter in strain gauge measurement was employed with a proper cutoff frequency to ensure closed loop stability. In [6] an adaptive control using sliding mode technique similar to [3] for a single link flexible manipulator is designed.

Intelligent control Methods

Soft computing techniques such as Fuzzy logic (FL), Neural Networks (NN), Reinforcement learning (RL) are also used in the control of flexible manipulators. The control with some intelligence is sometimes required to tackle unknown environment and to improve the whole performance of the system. These techniques are employed to choose suitable gains in feedforward compensation, feedback loop or both.

A vibration control using neural network was proposed in [4] for planar multilink flexible structures. In [9] a NN was developed to incrementally change the joint trajectory to achieve tip trajectory tracking in operational space. The tip position error was utilized as inputs to NN. The joint trajectory from NN was then controlled by PD control in joint space.

A cascade Fuzzy logic control (FLC) was proposed in [2] for a single link flexible manipulator. The control has a 3 FLCs, first fuzzy logic control has the input of joint position and derivate error, second FLC has tip position and derivate error. The first and second FLC outputs are the inputs to third FLC.

A Fuzzy-Neuro control was developed in [1] [2] for a planar two link rigidflexible manipulator. Fuzzy logic control was used in feedback loop and dynamic recurrent neural network (DRNN) was used in feedforward term. The parameter output from FLC is used to update the adaptive DRNN model. The controller was applied for first three vibration modes of flexible arm.

In [3] a composite controller was developed using singular perturbation approach.

The rigid body modes (slow dynamics) were controlled using NN and flexible modes (fast dynamics) were controlled using PD control. The proposed controller was compared with classical PD (slow dynamics)-PID (fast dynamics) control with additional frictional term. The composite controller showed good tracking in the presence of friction compared to PD-PID control. In [40] a fuzzy logic control using singular perturbation approach is proposed. Slow dynamics are controlled using fuzzy logic for joint trajectory tracking and fast dynamics are controlled using optimal LQR control to suppress vibrations.

In [9] a real time adaptive control was developed for a flexible manipulator carrying variable payload mass using reinforcement learning (RL). The performance of nonlinear adaptive control (NAC), fuzzy-based adaptive control (FBAC), reinforcement based adaptive control was compared for different payload mass. First nonlinear adaptive control was designed using linear-in parameter form similar to [7] with some arbitrary gains. These gains can produce stable trajectory tracking with the certain parameter range. To improve the performance of controller NAC for varying payload, a FL was used to choose appropriate gains with in parameter range. For FBAC, a prior knowledge on parameter range is required to assign suitable gains. To overcome this, RL based adaptive control was design. Actor-critic based RL adopts actor-critic weights according to payload variation. The experimental results showed that RL based adaptive control has good performance over FBAC and NAC for payload variation.

1.2 Research Objective

Many model based controllers were developed in the past for trajectory tracking and vibrations suppression. However, these are limited to numerical or experimental studies on planar flexible link manipulators. The current research will be focused to develop a systematic approach for the dynamic modeling and model based control design of spatial flexible manipulators.

The research activity on flexible manipulators is divided into two parts. The first part will be focused on dynamic modelling of spatial flexible manipulators while the second part will be focused on control design for trajectory tracking and vibration suppression.

1.2.1 Dynamic modelling of flexible manipulators

The contribution of this thesis will be to develop a general purpose multi-body code that can accurately model the link and joint flexibility in the manipulator dynamics. The dynamic formulation will be developed based on the principle of virtual work and recursive kinematic formulation. The deformation of each link is assumed to be due to both bending and torsion. The deformation of the joints is assumed to be due to pure torsion.

A spatial flexible manipulator will be considered to study the effect of link and joint flexibility on manipulator dynamics. The following cases are considered for the study:

- Rigid links and Rigid joints
- Flexible links and Rigid joints
- Flexible links and Fleixble joints

1.2.2 Control modelling of flexible manipulators

Many model based controllers were proposed for flexible manipulators for trajectory tracking applications. These are designed based on the control schemes available for linear and nonlinear dynamic systems. Some of them used a linearized dynamic model to simplify control design process and the linear control techniques to analyze system stability and robustness properties. The following control schemes are widely used to design control for flexible manipulator, i.e PID control, singular perturbation method, stable inversion method, robust control, adaptive control, pole placement method, output redefinition, lead-lag control, iterative learning method, sliding mode control, and intelligent controls such as Fuzzy Logic control and Neural Network control. However, these are limited to numerical or experimental studies on planar flexible link manipulators.

The contribution of this thesis is to study the advantages and disadvantages of well developed controllers for planar flexible link manipulators and these methods are extended and improved to spatial flexible link manipulators. The following controllers will be developed for spatial flexible link manipulator:

- PD Control
- Stable Inversion Control
- A Nonlinear Control
- Adaptive Control

2 Dynamic modeling

In this chapter a systematic approach for the dynamic modeling of flexible manipulator is presented. Rigid links, flexible links, and flexible joints are considered in the dynamic formulation. The kinematics of flexible links are derived using the floating reference formulation. The flexible links are deformable due to bending and torsion. The elastic deformations of flexible link due to bending is defined using the Euler-Bernoulli beam formulation. The inclusion of the dynamics due to link flexibility makes the robot manipulator a continuous system and require infinite degrees of freedom to estimate the dynamic parameters. It is not feasible to include infinite DOF in the dynamic model from the numerical simulations and control design point of view. Thus, the finite element method is used to discretize the flexible link to get the finite dimensional dynamic model.

The equations of motion are derived using the principle of virtual work in an absolute coordinate system for the general purpose implementation. Then, the set of equations in absolute coordinates is converted into relative or independent coordinates using the recursive kinematic formulations. The dynamic model that are derived using the principle of virtual work and finite element method considers the coupling effect of rigid body motion and elastic deformations of flexible link.

A general purpose multi-body code has been developed based on systematic approach that is presented for dynamic formulation of flexible manipulators. The input to the multi-body code are physical parameters of the flexible manipulator and the output is finite dimensional dynamic model of flexible manipulator. The multi-body code can be used for numerical simulation and control design purpose.

2.1 Kinematic Description

In this section, the kinematic equations that describe the position, velocity and acceleration of an arbitrary point is presented. A set of coordinate systems i.e. global coordinate system, body-fixed coordinate system, and floating coordinate system are used to derive the kinematic equations. The body-fixed coordinate system is used to define the translation and rotation of rigid link, where as a floating coordinate system is used to define the translation and rotation of flexible link. The general displacements of a point is described using Chasles theorem. It defines an arbitrary displacement as a sum of the translation of a point and a rotation along the axis of rotation.

According to Chasles theorem [7], the arbitrary displacement of a point can be defined as

$$r = R + Au \tag{2.1}$$

Where, $r = [r_x\, r_y\, r_z]^T$ is the global position vector of an arbitrary point, $R = [R_x\, R_y\, R_z]^T$ is the position vector of the body coordinate system. A is the coordinate transformation matrix, and $u = [\,\bar{u}_x \;\; \bar{u}_y \; \bar{u}_z]$ is the local position vector defined with respect to the body coordinate system.

The transformation matrix A is defined as

$$A = \begin{bmatrix} 2(\beta_0^2+\beta_1^2)-1 & 2(\beta_1\beta_2-\beta_0\beta_2) & 2(\beta 1\beta 3 \;+\; \beta 0\beta 2) \\ 2(\beta 1\beta 2 \;+\; \beta 0\beta 2) & 2(\beta_0^2+\beta_2^2)-1 & 2(\beta_2\beta_3-\beta_0\beta_1) \\ 2(\beta_1\beta_3-\beta_0\beta_2) & 2(\beta 2\beta 3 \;+\; \beta 0\beta 1) & 2(\beta_0^2+\beta_3^2)-1 \end{bmatrix} \tag{2.2}$$

Where, β_0, β_1, β_2, and β_3 are the Euler parameters. These quantities are defined as

$$\beta_0 = \cos\left(\frac{\beta}{2}\right) \tag{2.3}$$

$$\beta_1 = \upsilon_1 \sin(\frac{\beta}{2}) \tag{2.4}$$

$$\beta_2 = \upsilon_2 \sin(\frac{\beta}{2}) \tag{2.5}$$

$$\beta_3 = \upsilon_3 \left(\frac{\beta}{2}\right) \tag{2.6}$$

in which υ_1,υ_1, and υ_1 are components of the unit vector υ along the axis of rotation. β is the angle of rotation.

Using Chasles theorem, the kinematic equations for the position, velocity and acceleration of rigid and flexible links are derived.

2.1.1 Kinematics of Rigid link

The representation of an arbitrary point $\bar{O}_i$ on the rigid link i is shown in Figure 2.1. The kinematic equation that defines an arbitrary displacement of a rigid link i is derived using the body-fixed coordinate system. The body coordinate system $X_iY_iZ_i$ is attached to the rigid link i to identify the position and orientation of the rigid link i in space. The representation of an arbitrary point $\bar{O}_i$ on the rigid link i is shown in Figure 2.1.

The configuration of each point on the rigid link i in space can be described using the position and orientation of the body coordinate system $X_iY_iZ_i$ that are defined with respect to the global coordinate system $XY\,Z$.

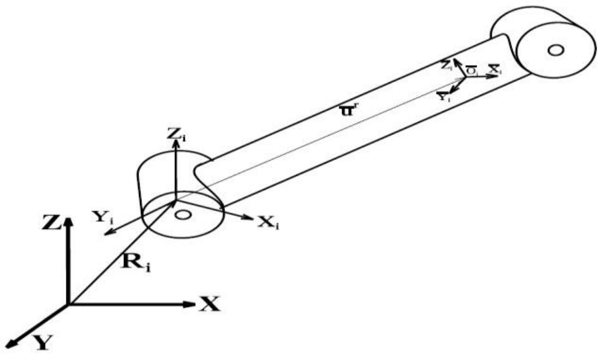

Figure 2.1 - Representation of an arbitrary point on a rigid link

The position vector of an arbitrary point on the rigid link *i* is defined as

$$r_i = R_i + A_i\bar{u}_i \tag{2.7}$$

where, $R_i = \left[R_x^i\ R_y^i\ R_z^i\right]^T$ is the position vector of the body coordinate system $X_iY_iZ_i$. A_i is the transformation matrix defined using equation (2.2), and $\bar{u}_i = \left[\bar{u}_x^i\ \ \bar{u}_y^i\ \ \bar{u}_z^i\right]^T$ is the local position vector defined with respect to $X_iY_iZ_i$. For the rigid link, the local position vector u_i is a constant vector.

The velocity vector of an arbitrary point on the rigid link *i* is obtained by differentiating equation (2.7). It is written as

$$\dot{r}_i = \dot{R}_i + A_i(\dot{\overline{w_i}} \times \bar{u}_i) \tag{2.8}$$

Where, $\bar{w}_i$is the angular velocity vector defined in the body coordinate system $X_iY_iZ_i$. It is expressed as

$$\bar{w}_i = \bar{G}_i\dot{\beta}_i \tag{2.9}$$

Where,

$$\bar{G} = 2 \times \begin{bmatrix} -\beta_1 & \beta_0 & \beta_3 & -\beta_2 \\ -\beta_2 & -\beta_3 & \beta_0 & \beta_1 \\ -\beta_3 & \beta_2 & -\beta_1 & \beta_0 \end{bmatrix} \tag{2.10}$$

Equation (2.8) is written in partitioned form as

$$\dot{r}_i = [I - A_i\tilde{\bar{u}}_i\bar{G}_i] \quad \begin{bmatrix} \dot{R}_i \\ \dot{\beta}_i \end{bmatrix} \tag{2.11}$$

The equation (2.11) can be written as

$$\dot{r}_i = L_i \dot{q}_i \tag{2.12}$$

Where,

$$L_i = [I - A_i \tilde{\bar{u}}_i \bar{G}_i], \tag{2.13}$$

$$\dot{q}_i = \begin{bmatrix} \dot{R}_i & \dot{\beta}_i \end{bmatrix}^T \tag{2.14}$$

in which $\dot{q}_i$ are the generalized velocities of the rigid link *i* defined in absolute coordinate system.

The acceleration vector of an arbitrary point on the rigid link *i* is obtained by differentiating equation (2.12). It is written as

$$\ddot{r}_i = L_i \ddot{q}_i + A_i (\tilde{\bar{\omega}}_i)^2 \bar{u}_i \tag{2.15}$$

Where,

$$\ddot{q}_i = \begin{bmatrix} \ddot{R}_i & \ddot{\beta}_i \end{bmatrix}^T \tag{2.16}$$

in which $\ddot{q}_i$ is the generalized accelerations of rigid link *i* defined in absolute coordinate system.

2.1.2 Kinematics of Flexible link

The representation of an arbitrary point $\bar{O}_i$ on the flexible link *i* is shown in Figure 2.2. The kinematic equations that can define an arbitrary displacement of a flexible link *i* is derived using floating reference frame formulation [7]. Floating reference frame formulation uses two sets of coordinates i.e., body reference coordinates and elastic coordinates. The body reference coordinates describe the position and orientation of body coordinate system $X_iY_iZ_i$ with respect to the global coordinate system $XY\,Z$. The elastic coordinates describe the local displacements of flexible link *i* with respect to the body coordinate system $X_iY_iZ_i$. The elastic deformations of flexible link are approximated using the finite element method to obtain finite set of elastic coordinates. The elastic coordinates of finite element shown in Figure 2.3 is defined using element coordinate system $X_{ij}Y_{ij}Z_{ij}$ with respect to body coordinate system $X_iY_iZ_i$. The position vector of an arbitrary point on flexible link *i* is defined as

$$r_i = R_i + A_i \bar{u}_i \tag{2.17}$$

where, $R_i = [R_xR_yR_z]^T$ is the position vector of the body coordinate system $X_iY_iZ_i$. A_i is the transformation matrix defined using equation (2.2), and u_i is the local position vector defined with respect to $X_iY_iZ_i$.

For the flexible link, the local position vector u_i is defined as the sum of undeformed position vector and elastic deformation vector. The local position vector u_i is written as

$$\bar{u}_i = \bar{u}_i^{\,r} + \bar{u}_i^{\,e} \tag{2.18}$$

Where, u^r_i is the undeformed position vector, and u^e_i is elastic deformation vector that is defined as

$$\bar{u}_i^{\,e} = S_i q_i^e \tag{2.19}$$

The representation of an arbitrary point $\bar{O}_i$ on the flexible link i is shown in Figure 2.2.

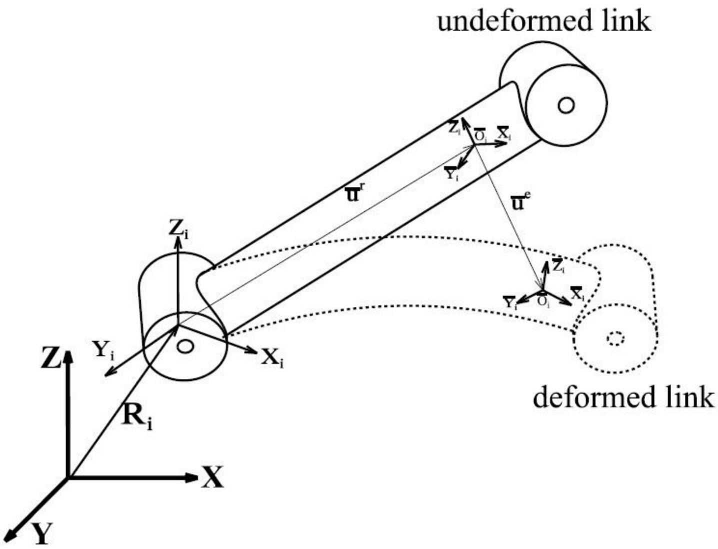

Figure 2.2 - Representation of an arbitrary point on a flexible link

The elastic coordinates of finite element shown in Figure 2.3.

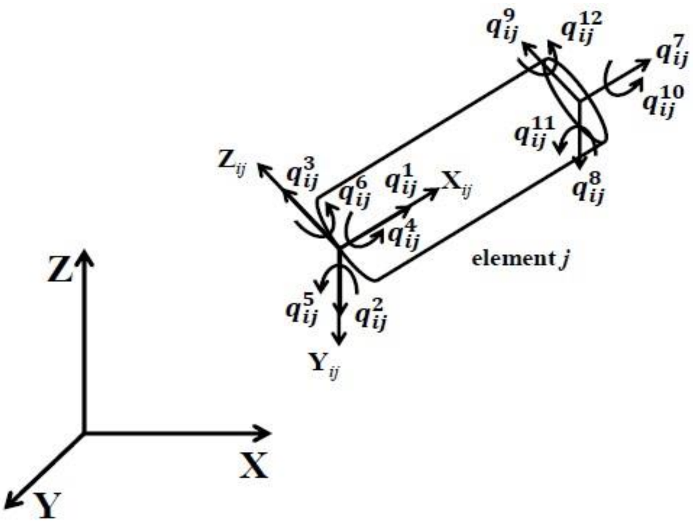

Figure 2.3 - Elastic coordinates on finite element

in which S_i is the shape function matrix, and q_i^e is the elastic coordinates vector. The shape function S_i is defined as

$$S_i = \begin{bmatrix} 1-\xi & 0 & 0 \\ 6(\xi-\xi^2)\eta & 1-3\xi^2+2\xi^3 & 0 \\ 6(\xi-\xi^2)\xi & 0 & 1-3\xi^2+2\xi^3 \\ 0 & -(1-\xi)\ell\zeta & (1-\xi)\ell\zeta \\ (1-4\xi+3\xi^2)\ell\zeta & 0 & (-\xi+2\xi^2-\xi^3)\ell \\ (-1+4\xi-3\xi^2)\ell\eta & (\xi-2\xi^2+\xi^3)\ell & 0 \\ \xi & 0 & 0 \\ 6(-\xi+\xi^2)\eta & 3\xi^2-2\xi^3 & 0 \\ 6(-\xi+\xi^2)\zeta & 0 & 3\xi^2-2\xi^3 \\ 0 & -\ell\xi\zeta & -\ell\xi\eta \\ (-2\xi+3\xi^2)\ell\zeta & 0 & (\xi^2-\xi^3)\ell \\ (2\xi-3\xi^2)\ell\eta & (-\xi^2+\xi^3)\ell & 0 \end{bmatrix} \tag{2.20}$$

$$\xi = \frac{u_x}{\ell}\ ;\ \frac{u_y}{\ell}\ ;\ \frac{u_z}{\ell}\ ; \tag{2.21}$$

Where, is length of element, and u_x,u_y,u_z are spatial coordinates along element axis.

The velocity vector of an arbitrary point on the flexible link i is obtained by differentiating equation (2.17). It is written as

$$\dot{r}_i = \dot{R}_i + A_i(\omega_i \times u_i) + A_i S_i \dot{q}_i^{e\ ggg} \tag{2.22}$$

Where, ω_i is angular velocity vector defined in body coordinate system $X_iY_iZ_i$. It is expressed as

$$\omega i = Gi\beta^{\cdot} I \; gggg \tag{2.23}$$

Where,

$$\bar{G} = 2 \times \begin{bmatrix} -\beta_1 & \beta_0 & \beta_3 & -\beta_2 \\ -\beta_2 & -\beta_3 & \beta_0 & \beta_1 \\ -\beta_3 & \beta_2 & -\beta_1 & \beta_0 \end{bmatrix} \tag{2.24}$$

Equation (2.22) is written in partitioned form as

$$\dot{r}_i = [I - A_i\tilde{\bar{u}}_i\bar{G}_i \quad A_iS_i \;] \quad \begin{bmatrix} \dot{R}_i \\ \dot{\beta}_i \\ \dot{q}_i^e \end{bmatrix} \tag{2.25}$$

The Equation (2.25) can be written as

$$\dot{r}_i = L_i\dot{q}_i \tag{2.26}$$

Where,

$$L_i = [I - A_i\tilde{\bar{u}}_i\bar{G}_i \qquad A_iS_i] \tag{2.27}$$

$$\dot{q}_i = \begin{bmatrix} \dot{R}_i & \dot{\beta}_i & \dot{q}_i^e & \end{bmatrix}^T \tag{2.28}$$

in which $\dot{q}_i$ is generalized velocities of flexible link *i* defined in absolute coordinate system.

The acceleration vector of an arbitrary point on the flexible link *i* is obtained by differentiating equation (2.26). It is written as

$$\ddot{r}_i = L_i\ddot{q}_i + A_i(\tilde{\bar{\omega}}_i)^2\bar{u}_i + 2A_i\tilde{\bar{\omega}}_iS_i\dot{q}_i^e \tag{2.29}$$

Where,

$$\ddot{q}_i = \begin{bmatrix} \ddot{R}_i & \ddot{\beta}_i & \ddot{q}_i^e & \end{bmatrix}^T \tag{2.30}$$

in which $\ddot{q}_i$ is generalized accelerations of the flexible link *i* defined in absolute coordinate system.

2.2 Dynamics description

The equations of motion are derived using the principle of virtual work in absolute coordinate system. In this section, the dynamic equations of rigid link, flexible link, and flexible joint are presented.

2.2.1 Rigid link modeling

The virtual work of total forces acting on rigid link i is defined as

$$\delta W_i = \delta W_i^i + \delta W_i^e \tag{2.31}$$

Where, δW_i^i, and δW_i^e are respectively the virtual work of inertia forces, and external forces.

The virtual work of inertia forces acting on rigid link i is written as

$$\delta W_i^i = \int_{V_i} \rho_i \, \ddot{r}_i^T \delta r_i dV_i \tag{2.32}$$

Where, ρ_i and V_i are respectively, the mass density and volume of rigid link ij; $\ddot{r}_i$ and δr_i are respectively the acceleration vector and virtual displacements of an arbitrary point on rigid link i.

The virtual displacement δr_i is written as

$$\delta r_i = L_i \delta q_i \tag{2.33}$$

Where,

$$L_i = [I - A_i \tilde{\bar{u}}_i \bar{G}_i], \tag{2.34}$$

$$\delta q_i = [\delta R_i \quad \delta \beta_i]^T \tag{2.35}$$

Where, q_i is generalized coordinates of rigid link i defined in absolute coordinate system. The acceleration vector $\ddot{r}_i$of an arbitrary point can be defined using equation (2.15). It is expressed as

$$\ddot{r}_i = L_i \ddot{q}_i + Q_i \tag{2.36}$$

in which $\ddot{q}_i$ is the generalized accelerations and Q_i is the quadratic term which is written as

$$Q_i = A_i (\tilde{\bar{\omega}}_i)^2 \bar{u}_i \tag{2.37}$$

Substituting acceleration vector $\ddot{r}_i$ and virtual displacements δr_i in equation (2.32) give

$$\delta W_i^i = \int_{V_i} \rho_i \, \ddot{q}_i^T L_i^T L_i \delta q_i dV_i + \int_{V_i} \rho_i \, . Q_i^T L_i \delta q_i dV_i \tag{2.38}$$

$$\delta W_i^i = \left[\ddot{q}_i^T \quad M_i - Q_i^{v^T}\right] \delta q_i \tag{2.39}$$

Where, M_i and Q_i^v are respectively the inertia matrix and quadratic velocity term.

$$M_i = \int_{V_i} \rho_i \begin{bmatrix} I & -A_i \; \tilde{\bar{u}}_i \, \bar{G}_i \\ -A_i \; \tilde{\bar{u}}_i \, \bar{G}_i & \bar{G}_i^T \tilde{\bar{u}}_i^T \, \tilde{\bar{u}}_i \, \bar{G}_i \end{bmatrix} dV_i \tag{2.40}$$

And

$$Q_i^v = -\int_{V_i} \rho_i \begin{bmatrix} I \\ -\bar{G}_i^T \tilde{\bar{u}}_i^T A_i^T \end{bmatrix} Q_i dV_i \tag{2.41}$$

The virtual work of external forces acting on rigid link *i* is defined as

$$\delta W_i^e = -Q_i^{e^T} \delta q_i \tag{2.42}$$

Substituting δW_i^i, and δW_i^e in equation (2.31) yields

$$\delta W_i = \left[\ddot{q}_i^T \quad M_i - Q_i^{v^T} - Q_i^{e^T}\right] q_{ij} \tag{2.43}$$

From equation (2.43) the equations of motion can be rearranged as

$$Mi\ddot{q}i = Qei + Qvi \tag{2.44}$$

Where, $Q^e{}_i$ and $Q^v{}_i$ are respectively the external forces applied and quadratic velocity term. Equation (2.44) is the equations of motion of rigid link in absolute coordinate system.

2.2.2 Flexible link modeling

The virtual work of total forces acting on flexible link *i* is defined as

$$\delta W_i = \delta W_i^i + \delta W_i^s + \delta W_i^e \tag{2.45}$$

Where, δW_i^i, δW_i^s, and δW_i^e are respectively the virtual work of inertia forces, elastic forces, and external forces acting on flexible link *i*. The flexible link *i* is discretized using finite element method to get finite dimensional dynamic model.

The representation of finite element *ij* on link *i* is shown in Figure 2.3. The virtual work of flexible link *i* can be obtained by summing up the virtual work of its elements.

The virtual work of total forces acting on element *ij* is defined as

$$\delta Wij = \delta Wiji + \delta Wijs + \delta Wije \qquad (2.46)$$

Where, $\delta W_{ij}{}^{i}$, $\delta W_{ij}{}^{s}$, and $\delta W_{ij}{}^{e}$ are respectively the virtual work of inertia forces, elastic forces, and external forces on element *ij*.

The virtual work of inertia forces acting on element *ij* is written as

$$\delta W_{ij}^{i} = \int_{V_{ij}} \rho_{ij}\, \ddot{r}_{ij}^{T} \delta r_{ij} d V_{ij} \qquad (2.47)$$

Where, ρ_{ij} and V_{ij} are respectively, the mass density and volume of element *ij*. $\ddot{r}_{ij}$ and δr_{ij} are respectively the acceleration vector and virtual displacements of an arbitrary point on element *ij*.

The virtual displacement δr_{ij} is written as

$$\delta r_{ij} = L_{ij} \delta q_{ij} \qquad (2.48)$$

Where,

$$L_{ij} = \begin{bmatrix} I - A_i \tilde{\bar{u}}_{ij} \bar{G}_i & A_i S_{ij} \end{bmatrix} \qquad (2.49)$$

$$\delta q_{ij} = \begin{bmatrix} \delta R_{ij} & \delta \beta_{ij} & \delta q^{e}{}_{ij} \end{bmatrix}^{T} \qquad (2.50)$$

Where, q_{ij} are the generalized coordinates of element *ij*.

The acceleration vector $\ddot{r}_{ij}$ of an arbitrary point can be defined using equation (2.29). It is expressed as

$$\ddot{r}_{ij} = L_{ij} \ddot{q}_{ij} + Q_{ij} \qquad (2.51)$$

Where,

$$\ddot{q}_{ij} = \begin{bmatrix} \ddot{R}_{ij} & \ddot{\beta}_{ij} & \ddot{q}_{ij}^{e} \end{bmatrix}^{T} \qquad (2.52)$$

And

$$Q_{ij} = A_i (\tilde{\bar{\omega}}_i)^2 \bar{u}_{ij} = 2 A_i \tilde{\bar{\omega}}_i S_{ij} \dot{q}_{ij}^{e} \qquad (2.53)$$

in which $\ddot{q}_{ij}$ are the generalized accelerations, and Q_{ij} is the quadratic term.

Substituting acceleration vector $\ddot{r}_{ij}$ and virtual displacements δr_{ij} in equation (2.47) gives

$$\delta W_{ij}^{i} = \int_{V_{ij}} \rho_{ij}\, \ddot{q}_{ij}^{T} L_{ij}^{T} L_{ij} \delta q_{ij} dV_{ij} + \int_{V_{ij}} \rho_{ij} \,.\, Q_{ij}^{T} L_{ij} \delta q_{ij} dV_{ij} \tag{2.54}$$

$$\delta W_{ij}^{i} = \left[\ddot{q}_{ij}^{T}\ M_{ij} - Q_{ij}^{v^{T}}\right] \delta q_{ij} \tag{2.55}$$

Where, M_{ij} and. Q_{ij}^{v} are respectively the inertia matrix and quadratic velocity term.

$$M_{ij} = \int_{V_{ij}} \rho_{ij} \begin{bmatrix} I & -A_i\ \tilde{\bar{u}}_{ij}\ \bar{G}_i & A_i S_{ij} \\ & & \bar{G}_i^{\,T} \tilde{\bar{u}}_{ij}^{\,T} S_{ij} \\ symmetric & \bar{G}_i^{\,T} \tilde{\bar{u}}_{ij}^{\,T} \tilde{\bar{u}}_{ij}\ \bar{G}_i & S_{ij}^{T} S_{ij} \end{bmatrix} dV_{ij} \tag{2.56}$$

$$Q_{ij}^{v} = -\int_{V_{ij}} \rho_{ij} \begin{bmatrix} I \\ -\bar{G}_i^{\,T} \tilde{\bar{u}}_{ij}^{T} A_i^{T} \\ S_{ij}^{T} A_i^{T} \end{bmatrix} Q_{ij} dV_{ij} \tag{2.57}$$

and

The virtual work of elastic forces due to the deformation of element *ij* can be defined as

$$\delta W_{ij}^{s} = -\int_{V_{ij}} \sigma_{ij}^{T} \delta \varepsilon_{ij} dV_{ij} \tag{2.58}$$

where, σ_{ij} and ε_{ij} are respectively the stress and the strain vectors of element *ij*.

$$\varepsilon_{ij} = D_{ij} \bar{u}_{ij}^{e} = D_{ij} S_{ij} q_{ij}^{e} \tag{2.59}$$

$$\sigma_{ij} = E_{ij} \varepsilon_{ij} = E_{ij} D_{ij} S_{ij} q_{ij}^{e} \tag{2.60}$$

Substituting equation (2.59) and (2.60) in equation (2.58) gives

$$\delta W_{ij}^{s} = -q_{ij}^{e\,T} \left[\int_{V_{ij}} \left(D_{ij} S_{ij}\right)^{T} E_{ij} D_{ij} S_{ij} dV_{ij} \right] \delta q_{ij}^{e} = -q_{ij}^{e\,T} K_{ij}^{e} \delta q_{ij}^{e} \tag{2.61}$$

Where, K_{ij}^{e} is the element stiffness matrix defined as.

$$K_{ij}^{e} = \int_{V_{ij}} \left(D_{ij}S_{ij}\right)^{T} E_{ij}D_{ij}S_{ij}dV_{ij} \tag{2.62}$$

in which D_{ij} is the differential operator, S_{ij} is the element shape function matrix and E_{ij} is the elastic coefficient.

The virtual work of external forces acting on element *ij* is defined as

$$\delta W_{ij}^{e} = -{Q_{ij}^{e}}^{T}\delta q^{i} \tag{2.63}$$

Substituting ${\delta W_{ij}}^{i}$, ${\delta W_{ij}}^{s}$ and ${\delta W_{ij}}^{e}$ in equation (2.46) fields

$$\delta W_{ij} = \left[\ddot{q}_{ij}^{T}M_{ij} - {Q_{ij}^{v}}^{T} - {q_{ij}^{e}}^{T}K_{ij}^{e} - {Q_{ij}^{e}}^{T}\right]\delta q_{ij} \tag{2.64}$$

From equation (2.64) the equations of motion can be rearranged as

$$M_{ij}\ddot{q}_{ij} = Q_{ij}^{e} + Q_{ij}^{v} + Q_{ij}^{s} \tag{2.65}$$

Where, Q_{ij}^{e} are the applied external forces. Q_{ij}^{v} and Q_{ij}^{s} are respectively the quadratic velocity term and elastic forces acting on element *ij*.

The virtual work of total forces acting on flexible link *i* is defined as

$$\delta W_{i} = \sum_{j=1}^{n_e} {\delta W_{ij}}^{i} + \sum_{j=1}^{n_e} {\delta W_{ij}}^{s} + \sum_{j=1}^{n_e} {\delta W_{ij}}^{e} \tag{2.66}$$

Where, n_e is the number of finite elements.

Equation (2.65) can be extended to all finite elements in flexible link *i* and assembled based on element connectivity to form a dynamic model of flexible link.

Using the equation (2.66), the equations of motion of the flexible link *i* is defined as

$$M_{i}\ddot{q}_{i} = Q_{i}^{e} + Q_{i}^{v} + Q_{i}^{s} \tag{2.67}$$

Where, Q_{i}^{e} are the external forces applied on flexible link *i*. Q_{i}^{v} and Q_{i}^{s} are respectively the quadratic velocity term and elastic forces acting on flexible link *i*.

The equations of motion in absolute coordinate system for *n* link manipulator can be defined as

$$\begin{bmatrix} M_1 & 0 & \cdots & 0 \\ 0 & M_2 & \dots & 0 \\ \vdots & \vdots & \ddots & 0 \\ 0 & 0 & 0 & M_n \end{bmatrix} \begin{bmatrix} \ddot{q}_1 \\ \ddot{q}_2 \\ \cdots \\ \ddot{q}_n \end{bmatrix} = \begin{bmatrix} Q_1^e \\ Q_2^e \\ \cdots \\ Q_n^e \end{bmatrix} + \begin{bmatrix} Q_1^v \\ Q_2^v \\ \cdots \\ Q_n^v \end{bmatrix} + \begin{bmatrix} Q_1^s \\ Q_2^s \\ \cdots \\ Q_n^s \end{bmatrix} \tag{2.68}$$

The equation (2.68) expressed in compact form as

$$\bar{M}\ddot{\bar{q}} = \bar{Q}^e + \bar{Q}^v + \bar{Q}^s \tag{2.69}$$

Where,

$$\bar{M} = \begin{bmatrix} M_1 & 0 & \cdots & 0 \\ 0 & M_2 & \dots & 0 \\ \vdots & \vdots & \ddots & 0 \\ 0 & 0 & 0 & M_n \end{bmatrix} \tag{2.70}$$

$$\ddot{\bar{q}} = [\ddot{q}_1 \; \ddot{q}_2 \; \dots \; \ddot{q}_n \,]^T \tag{2.71}$$

$$\bar{Q}^e = [Q_1^e \;\; Q_2^e \;\; \dots \; Q_n^e \,]^T \tag{2.72}$$

$$\bar{Q}^v = [Q_1^v \;\; Q_2^v \;\; \cdots \; Q_n^v \,]^T \tag{2.73}$$

$$\bar{Q}^s = [Q_1^s \;\; Q_2^s \;\; \cdots \; Q_n^s]^T \tag{2.74}$$

The equation [2.68] is the dynamic model derived in absolute coordinates. The relative motions between the flexible links are imposed using recursive kinematic formulation. The recursive kinematic formulation is presented in section (2.3)

2.2.3 Flexible joint modeling

The revolute joint *j* with actuator and transmission system is shown in Figure (2.4). The actuator is assumed as electric motor and torsional spring represents the flexibility induced due to the transmission system. θ_j and θ_i respectively are the rotations of actuator *j* and link *i*.

The virtual work of torque exserted on link *i* by actuator *j* and transmission system is defined as

$$\delta W_j = T\,\delta\theta_{ij} \tag{2.75}$$

Where, T is the total torque acting at the joint. The equation (2.75) is written in explicit form as

$$\delta W_j = (J_j + \ddot{\theta}_j + C_j(\dot{\theta}_j - \dot{\theta}_i) + K_j(\dot{\theta}_j - \dot{\theta}_i) - T_j)\delta\theta_{ij} \tag{2.76}$$

The revolute joint j with actuator and transmission system is shown in Figure 2.4.

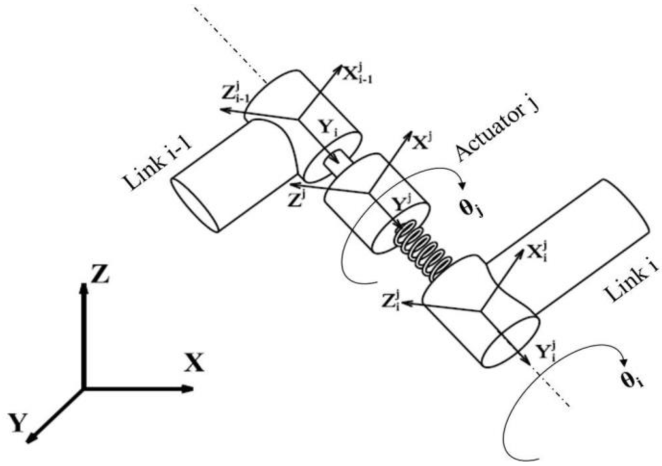

Figure 2.4 - Flexible joint j assembly

Where, J_j is the inertia of the motor. K_j and C_j are the stiffness and damping coefficients of the transmission system. T_j is the torque produced by motor. $\delta\theta_{ij}$ is the virtual change at joint. The equations of motions of joint assembly is written as

$$(J_j\ddot{\theta}_j + C_j(\dot{\theta}_j - \dot{\theta}_i) + K_j(\dot{\theta}_j - \dot{\theta}_i) = Tj \tag{2.77}$$

2.3 Recursive Kinematic Formulation

Consider two flexible link $i - 1$ and i shown in Figure 2.5 which are connected by a revolute joint j. The joint allows relative rotation along joint axis and has one rigid body coordinates θ_i.

The following kinematic relationship for revolute joint holds the relation between generalized coordinates and joint coordinates [6]

$$R_i + A_i\bar{u}_i^j - R_{i-1} - A_{i-1}\bar{u}_{i-1}^j = 0 \tag{2.78}$$

$$\omega_i = \omega_{i-1} + \omega_{i-1}^j - \omega_i^j + \omega_{i,i-1} \tag{2.79}$$

Where, $\bar{u}_i^j$ and$\bar{u}_{i-1}^j$ are local position vectors of joint defined on link *i* and *i*−1 respectively. ω_i^j andω_{i-1}^j are respectively the local angular velocity vectors of joint due to elastic deformations on link *i* and *i* − 1. These vector quantities are defined as

$$\omega_{i-1}^j = A_{i-1} S_{i-1}^{jr} \dot{q}_{i-1}^e \tag{2.80}$$

$$\omega_{ij} = A_i S_{ijr} \dot{q}_{ie} \tag{2.81}$$

in which S_i^{jr} and S_{i-1}^{jr} are respectively the constant shape function matrix of joint rotations due to elastic deformations on link *i* and *i* − 1. $\omega_{i,i-1}$ is relative angular velocity vector of link *i* with respect to link *i-1* is expressed as

$$\omega_{i,i-1} = \nu_{i-1} \dot{\theta}_i \tag{2.82}$$

Consider two flexible link *i* − 1 and *i* shown in Figure (2.5).

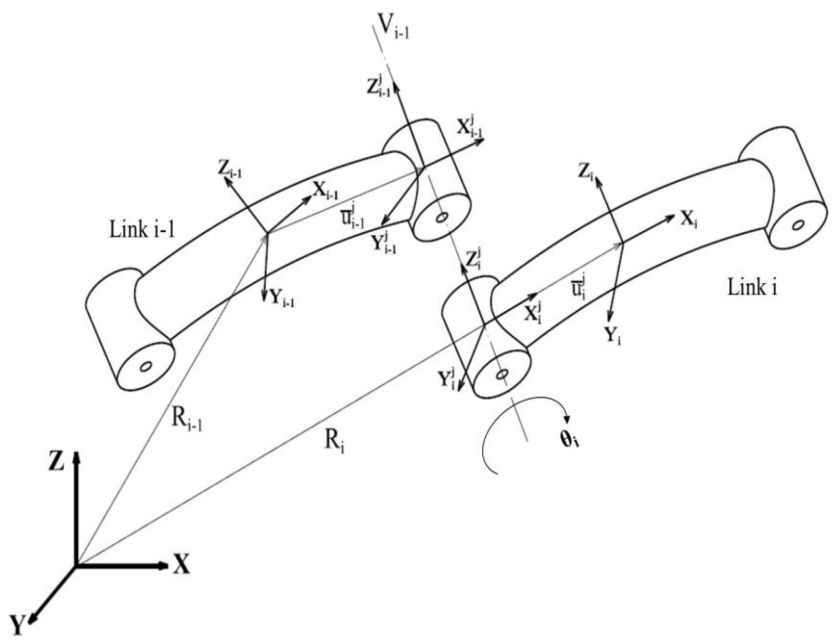

Figure 2.5 - Representation of Relative body Coordinates

Where, ν_{i-1} is rotation axis defined with respect to link *i*−1 in global coordinate system *XY Z*.

$$\nu_{i-1} = A_{i-1} \bar{\nu}_{i-1} \tag{2.83}$$

ν_{i-1} is constant vector defined with respect to link $i-1$ in body coordinate system $X_{i-1}Y_{i-1}Z_{i-1}$.

Differentiating equation (2.78) twice with respect to time and equation (2.79) once with respect to time gives

$$\begin{aligned}\ddot{R}_i - A_i\tilde{\bar{u}}_i^j\bar{G}_i\ddot{\beta}_i + A_iS_i^{jt}\ddot{q}_i^e = \\ = \ddot{R}_{i-1} - A_{i-1}\tilde{\bar{u}}_{i-1}^j\bar{G}_{i-1}\ddot{\beta}_{i-1} + A_{i-1}S_{i-1}^{jt}\ddot{q}_{i-1}^e + \gamma R\end{aligned} \tag{2.84}$$

$$\dot{\omega}_i = \dot{\omega}_{i-1} + A_{i-1}S_{i-1}^{jr}\ddot{q}_{i-1}^e - A_iS_i^{jr}\ddot{q}_i^e + A_{i-1}\bar{v}_{i-1}\ddot{\theta}_i + \gamma\beta \tag{2.85}$$

Where, S_i^{jt} andS_{i-1}^{jt} are respectively the shape functions of joint translations defined on link *i* and *i-1*. γ_R and γ_β are written as

$$\begin{aligned}\gamma R = -A_i(\tilde{\bar{\omega}}_i)^2\bar{u}_i^j = \\ A_{i-1}(\tilde{\bar{\omega}}_{i-1})^2\bar{u}_{i-1}^j - 2A_i\tilde{\bar{\omega}}_iS_i^{jt}\dot{q}_i^e + 2A_{i-1}\tilde{\bar{\omega}}_{i-1}S_{i-1}^{jt}\dot{q}_{i-1}^e\end{aligned} \tag{2.86}$$

$$\gamma\beta = A_{i-1}\tilde{\bar{\omega}}_{i-1}\bar{v}_{i-1}\dot{\theta}_i + A_{i-1}\tilde{\bar{\omega}}_{i-1}S_{i-1}^{jr}\dot{q}_{i-1}^e - A_i\tilde{\bar{\omega}}_iS_i^{jr}\dot{q}_i^e \tag{2.87}$$

The equation [2.84] and [2.85] can be written in a compact form as

$$D_i\ddot{q}_i = D_{i-1}\ddot{q}_{i-1} + H_i\ddot{P}_i + \gamma_i \tag{2.88}$$

Where,

$$D_i = \begin{bmatrix} I & -A_i\tilde{\bar{u}}_i^j\bar{G}_i & A_iS_i^{jt} \\ 0 & A_i\bar{G}_i & A_iS_i^{jr} \\ 0 & 0 & I \end{bmatrix} \tag{2.89}$$

$$D_{i-1} = \begin{bmatrix} I & -A_{i-1}\tilde{\bar{u}}_{i-1}^j\bar{G}_{i-1} & A_{i-1}S_{i-1}^{jt} \\ 0 & A_{i-1}\bar{G}_{i-1} & A_{i-1}S_{i-1}^{jr} \\ 0 & 0 & 0 \end{bmatrix} \tag{2.90}$$

$$H_i = \begin{bmatrix} A_{i-1}\bar{v}_{i-1} & 0 \\ 0 & I \end{bmatrix} \tag{2.91}$$

$$\ddot{P}_i = [\ddot{\theta}_i \quad \ddot{q}_i^e]^T \tag{2.92}$$

$$\gamma^i = [\gamma_R \quad \gamma_\beta]^T \tag{2.93}$$

The generalization of recursive kinematic formulation for a n link manipulator is expressed as

$$\begin{bmatrix} D_1 & 0 & \cdots & 0 \\ -D_1 & D_2 & \dots & 0 \\ \vdots & \vdots & \ddots & 0 \\ 0 & 0 & -D_{n-1} & D_n \end{bmatrix} \begin{bmatrix} \ddot{q}_1 \\ \ddot{q}_2 \\ \cdots \\ \ddot{q}_n \end{bmatrix} = \begin{bmatrix} H_1 & 0 & \cdots & 0 \\ 0 & H_2 & \dots & 0 \\ \vdots & \vdots & \ddots & 0 \\ 0 & 0 & 0 & H_n \end{bmatrix} \begin{bmatrix} \ddot{P}_1 \\ \ddot{P}_2 \\ \cdots \\ \ddot{P}_n \end{bmatrix} + \begin{bmatrix} \gamma_1 \\ \gamma_2 \\ \cdots \\ \gamma_n \end{bmatrix} \tag{2.94}$$

The equation (2.94) can be written in compact form as

$$\bar{D}\ddot{\bar{q}} = \bar{H}\ddot{\bar{P}} + \bar{\gamma} \tag{2.95}$$

$$\overline{D = \begin{bmatrix} D_1 & 0 & \cdots & 0 \\ -D_1 & D_2 & \dots & 0 \\ \vdots & \vdots & \ddots & 0 \\ 0 & 0 & -D_{n-1} & D_n \end{bmatrix}} \tag{2.96}$$

$$\ddot{\bar{q}} = [\ddot{q}_1 \; \ddot{q}_2 \; \dots \; \ddot{q}_n \,]^T \tag{2.97}$$

$$\begin{bmatrix} H_1 & 0 & \cdots & 0 \\ 0 & H_2 & \dots & 0 \\ \vdots & \vdots & \ddots & 0 \\ 0 & 0 & 0 & H_n \end{bmatrix} \tag{2.98}$$

$$\ddot{\bar{P}} = \left[\ddot{P}_1 \; \ddot{P}_2 \; \dots \; \ddot{P}_n \,\right]^T \tag{2.99}$$

$$\ddot{\bar{\gamma}} = [\gamma_1 \; \gamma_2 \; \dots \; \gamma_n \,]^T \tag{2.100}$$

The generalized accelerations of n link manipulator $\ddot{\bar{q}}$ in absolute coordinate system can be expressed in terms of relative or independent coordinates as

$$\ddot{\bar{q}} = \bar{B}\ddot{\bar{P}} + \tilde{\gamma} \tag{2.101}$$

Where,

$$\bar{B} = \bar{D}^{-1}\bar{H} \tag{2.102}$$

$$\tilde{\gamma} = \bar{D}^{-1}\bar{\gamma} \tag{2.103}$$

Substituting the generalized acceleration $\ddot{q}$ in equation (2.69) and premultiplying with B gives the dynamic model of n link manipulator in relative or independent coordinates form. It is written as

$$\bar{B}^T \bar{M} \bar{B} \ddot{P}_i = \bar{B}^T (\bar{Q}^e + \bar{Q}^v + \bar{Q}^s - \bar{M}\tilde{\gamma}) \tag{2.104}$$

The equation (2.105) is a coupled and nonlinear dynamic model of n link manipulator which can be used for numerical simulation and model based control which is written as

$$M\ddot{P} = Q \tag{2.105}$$

Where,

$$M = \bar{B}^T \bar{M} \bar{B} \tag{2.106}$$

$$Q = \bar{B}^T (\bar{Q}^e + \bar{Q}^v + \bar{Q}^s - \bar{M}\tilde{\gamma}) \tag{2.107}$$

design purpose.

2.4 Multi-Body Code Structure

A gerneral purpose multi-body code has been developed in MATLAB to get the dynamic model for numerical simulation and model based control design purpose. The structure of the multi-body code is shown in Figure 2.6. The input to the multibody code consists of physical parameters of body, joint, and actuators. The dynamic model is nonlinear and configuration dependent. Hence, to get the dynamic parameters such as inertia matrix, coriolis and centrifugal matrix, stiffness matrix, and damping matrix the position and velocities of manipulator links are necessary. In the multi-body code the damping matrix is defined using Rayleigh damping. Overall the input file format consists of body definition, joint definition, actuator definition, position vector and velocity vector of the manipulator.

The structure of the multi-body code is shown in Figure 2.6.

Body definition

The body definition is declared as a MATLAB structure called body structure. The input fields to the body structure is shown in Table [2.1]. The body structure contains all the necessary fields that are required for dynamic modeling. The user can choose the rigid link modeling or flexible link modeling in the structure input field "body".

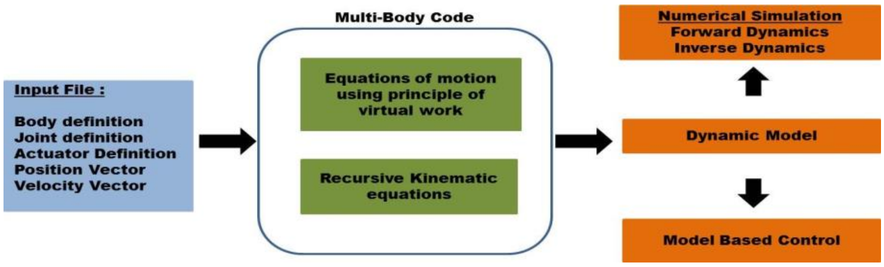

Figure 2.6 - The structure of the multi-body code

Table 2.1 - The input fields of body structure

Field	Input Format	Description
name	String	Input to assign name to the body
body	Number	1 = Rigid link / 2 = Flexible link
element	Number	Number of finite element to discretize the link (1 - for rigid link, n - for flexible link)
density	Number	Density of the link (Kg/m^3)
youngs_mod	Number	Youngs Modulus of the link (MPa)
shear_mod	Number	Shear Modulus of the link (MPa)
moment_inertia	Number	Area Moment of Inertia (m^4)
polar_inertia	Number	Moment of Inertia (m^4)
length	Number	Length of the link (m)
area	Number	Cross-section area (m^2)
alpha	Number	Rayleigh Damping constant
beta	Number	Rayleigh Damping constant

Joint definition

The joint definition is declared as a MATLAB structure called joint structure. The input fields to the joint structure is shown in Table 2.2. The user can choose the rigid joint or flexible joint modeling in the structure input field "joint". In the joint structure, inertia, damping, and stiffness properties are considered to model dynamics of flexible joint. The flexible joint is necessary for the modeling of flexible joint manipulator such as KUKA-DLR light weight manipulator.

Table 2.2 - The input fields of joint structure

Field	Input Format	Description
name	String	Input to assign name to the joint
joint	Number	1 = rigid joint ; 2 = flexible joint;
inertia	Number	Inertia of the motor

Table continuation 2.2

stiff	Number	Stiffness of the joint
damp	Number	Damping of the joint
axis	Number	1 = X-axis; 2 = Y-axis; 3 = Z-axis;
body1	Number	Link number
body2	Number	Link number
body1_frame	Vector	Joint location w.r.t body1
body2_frame	Vector	Joint location w.r.t body2

Actuator definition

The actuator definition is declared as a MATLAB structure called actuator structure. The actuator structure is optional choice. It is particularly useful for forward dynamic simulation. The input fields to the actuator structure is shown in Table 2.3.

Table 2.3 - The input fields of actuator structure

Field	Input Format	Description
name	String	Input to assign name to the actuator
load	Number	Input torque (N-m)
axis	Number	1 = X-axis; 2 = Y-axis; 3 = Z-axis;
body1	Number	Link number
body2	Number	Link number

2.5 Study of flexibility effects on spatial manipulator

A spatial RRR manipulator shown in Figure 2.7, is considered to demonstrate the effect of link and joint flexibility on manipulator dynamics. The physical parameters of a RRR spatial manipulator is presented in Table 2.4. Uniform cross-section and material properties are assumed on each link.

Table 2.4 - The physical parameters of a RRR flexible manipulator

Parameter	Link 1	Link 2	Link 3
Link Length (m)	1	4.0	3.5
C/s Area (m^2)	0.028	0.0020	0.0008
Moment of Inertia (m^4)	8.33×10^{-7}	6.24×10^{-7}	5.37×10^{-7}
Polar moment of Inertia (m^4)	1.66×10^{-6}	1.24×10^{-6}	1.07×10^{-6}
Density (Kg/m^3)		8253	

A spatial RRR manipulator shown in Figure 2.7.

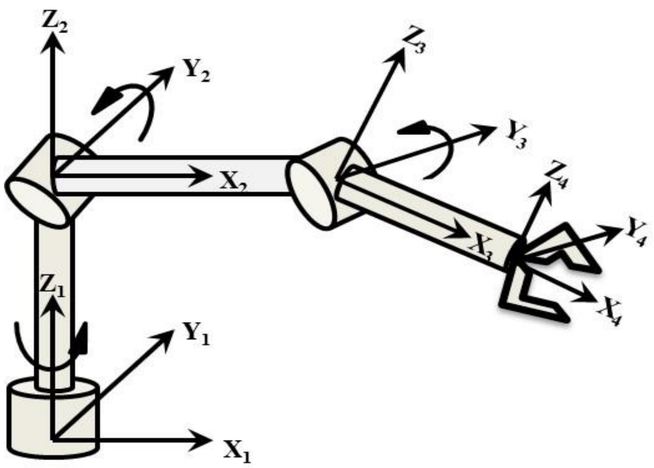

Figure 2.7 - Spatial RRR flexible manipulator

The following cases are considered to study the effect of flexibility on RRR spatial manipulator dynamics:

- Rigid links and Rigid joints
- Flexible links and Rigid joints
- Flexible links and Fleixble joints

Each flexible link is discretized using two finite element beams with six degrees of freedom on each node and one degree of freedom for rigid body rotations, i.e. θ_i where i = 1,2,3. Manipulator joint has one rigid body rotation, i.e. θ_j where j = 1,2,3. The torsional stiffness K_j for j = 1,2,3 at manipulator joints is defined as 5000 Nm/rad. The damping effects on links and joints are ignored in the numerical simulation.

2.5.1 Simulation results

A constant torque of 400 Nm, is applied at each manipulator joint for each case to compare manipulator endeffector $X_4Y_4Z_4$ motion. The endeffector $X_4Y_4Z_4$ motion in global coordinate system along the X,Y and Z direction is shown in Figure 2.8, 2.10. The elastic displacements of manipulator endeffector $X_4Y_4Z_4$ along the X,Y and Z direction is shown in Figure 2.11 - Figure 2.13. It shows the elastic displacements of flexible manipulator (i.e. Flexible links and Rigid joints, Flexible links and Fleixble joints) endeffector $X_4Y_4Z_4$ with respect to the rigid manipulator (i.e. Rigid links and Rigid joints) endeffector $X_4Y_4Z_4$ motion.

The joint response of RRR manipulator along joint 1, joint 2 and joint 3 is shown in Figure 2.8 - Figure 2.10. The joint deformations of flexible manipulator (i.e.

The endeffector $X_4Y_4Z_4$ motion in global coordinate system along the X,Y and Z direction is shown in Figure 2.8.

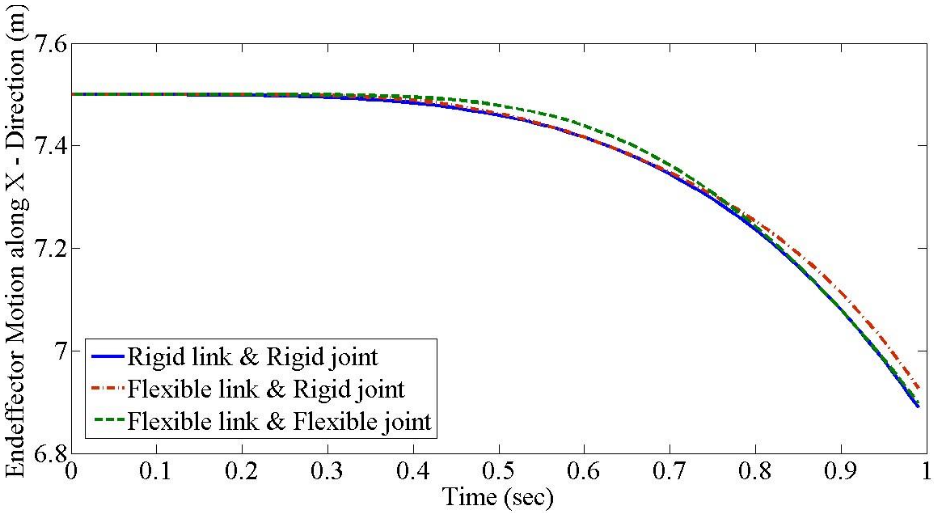

Figure 2.8 - Endeffector $X_4Y_4Z_4$ trajectory response along X-direction

Flexible links and Rigid joints, Flexible links and Fleixble joints) with respect to rigid manipulator joint motion is shown in Figure 2.17 - Figure 2.19.

In addition to link flexibility, the flexibility at manipulator joint can significantly alter the motion of the manipulator joint and eventually effects the endeffector $X_4Y_4Z_4$ motion. For the long reach manipulators having link dimensions in the order of few meters, the small elastic deformation at manipulator joint can lead to large endeffector position error. It is particulary evident in Figure 2.11 - Figure 2.13.

The numerical simulation results show that the link and joint flexibility can significantly alter the overall manipulator endeffector motion. Hence it is necessary to include the dynamics of link and joint flexibility to accurately represent the dynamic behaviour of the system.

The joint response of RRR manipulator along joint 1, joint 2 and joint 3 is shown in Figure 2.9.

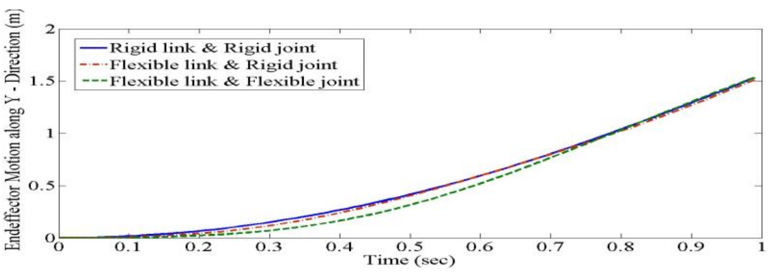

Figure 2.9 - Endeffector $X_4Y_4Z_4$ trajectory response along Y-direction

The joint response of RRR manipulator along joint 1, joint 2 and joint 3 is shown in Figure 2.10.

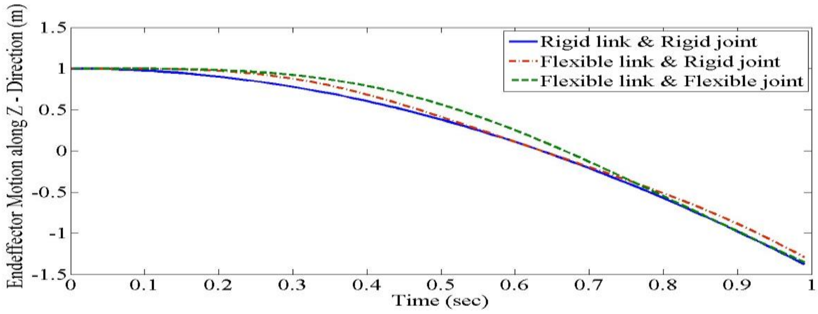

Figure 2.10 - Endeffector $X_4Y_4Z_4$ trajectory response along Z-direction

. For the long reach manipulators having link dimensions in the order of few meters shown in Figure 2.11.

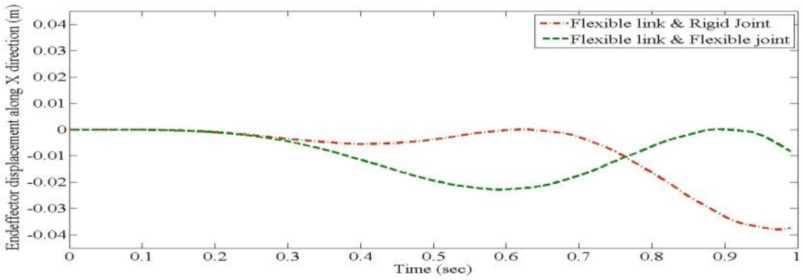

Figure 2.11- Elastic displacements of endeffector $X_4Y_4Z_4$ with respect to rigid manipulator endeffector motion in X-direction

The small elastic deformation at manipulator joint can lead to large endeffector position error shown in Figure 2.12.

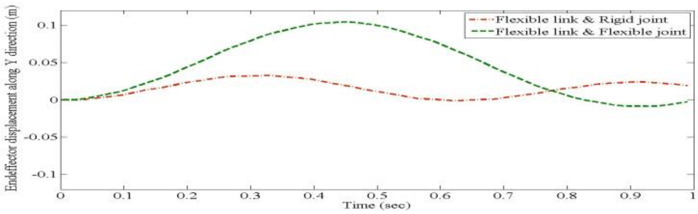

Figure 2.12 - Elastic displacements of endeffector $X_4Y_4Z_4$ with respect to rigid manipulator endeffector motion in Y-direction

Elastic displacements of endeffector $X_4Y_4Z_4$ with respect to rigid manipulator endeffector motion in Z-direction shown in Figure 2.13.

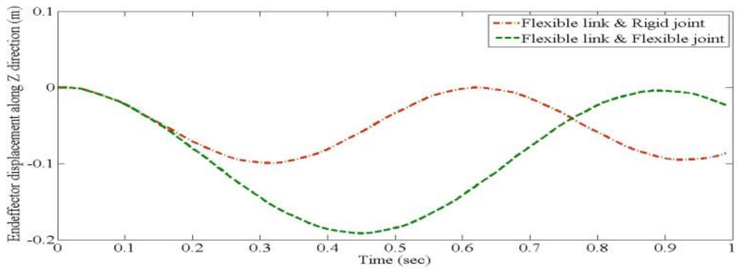

Figure 2.13 - Elastic displacements of endeffector $X_4Y_4Z_4$ with respect to rigid manipulator endeffector motion in Z-direction

Joint θ_1 trajectory response shown in Figure 2.14.

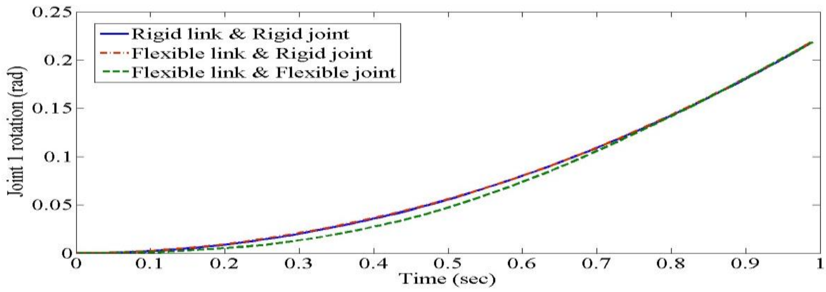

Figure 2.14 - Joint θ_1 trajectory response.

Joint θ_2 trajectory response shown in Figure 2.15.

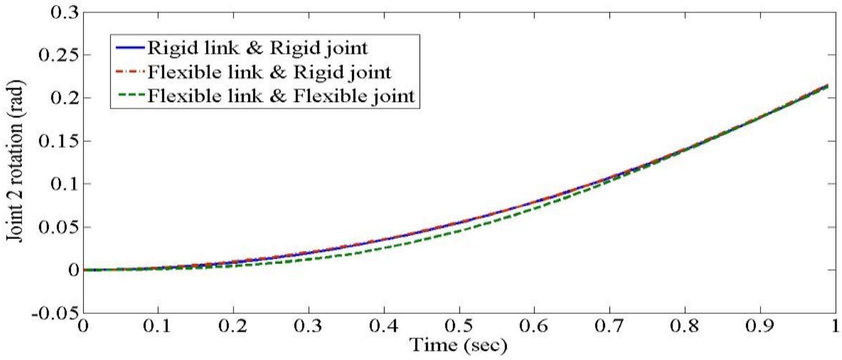

Figure 2.15 - Joint θ_2 trajectory response

Joint θ_3 trajectory response shown in Figure 2.16.

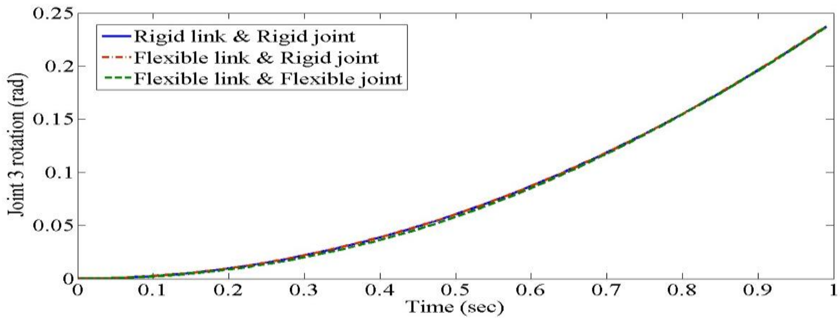

Figure 2.16 - Joint θ_3 trajectory response

Elastic deformations of joint θ_1 with respect to rigid manipulator joint motion shown in Figure 2.17.

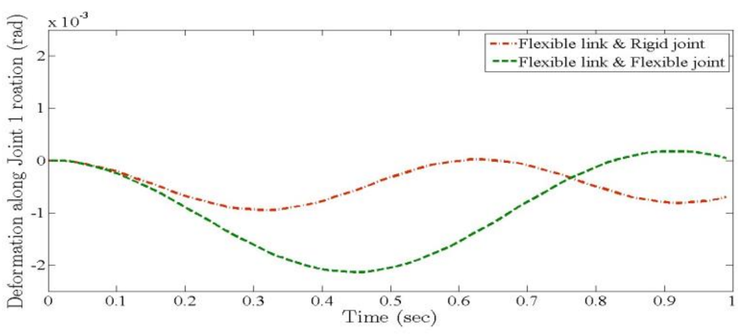

Figure 2.17 - Elastic deformations of joint θ_1 with respect to rigid manipulator joint motion

Elastic deformations of joint θ_2 with respect to rigid manipulator joint motion shown in Figure 2.18.

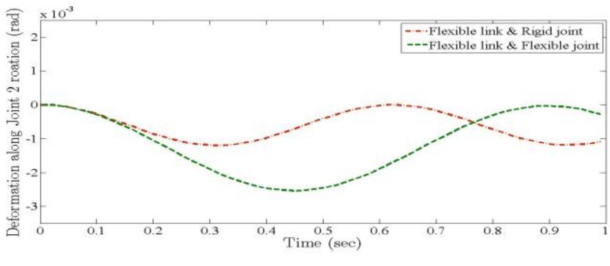

Figure 2.18 - Elastic deformations of joint θ_2 with respect to rigid manipulator joint motion

Elastic deformations of joint θ_3 with respect to rigid manipulator joint motion shown in in Figure 2.19.

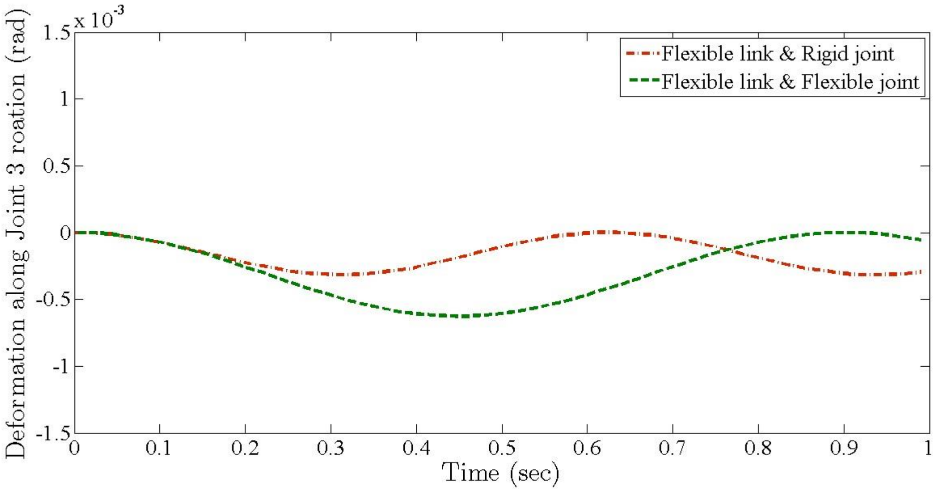

Figure 2.19 - Elastic deformations of joint θ_3 with respect to rigid manipulator joint motion

3 Control of flexible manipulators

Motion control of robot manipulator is important to achieve high speed operations and multi-functionality. In that, dynamic model identification and control are two subsets which are important to attain desired performance. In the previous chapter, the dynamic formulation is presented to identify the dynamic model based on physical parameters of the manipulator. In this chapter, model based control for trajectory tracking of spatial flexible manipulator is presented.

The objective of trajectory tracking control in the case of flexible manipulators is to follow the desired reference trajectory and minimize vibrations of the end-effector along trajectory. The approach to design a model based controller in order to meet the desired performance varies based on the type of flexibility in the system. Link flexibility is considered as most difficult to control because the flexibility is distributed and has infinite degrees of freedom. In this chapter, the controller design is mainly addressed for flexible link manipulators.

The most challenging problem in design of controller for flexible link manipulators is under actuation and non-minimal phase nature. Under actuation is due to finite number of actuators to control infinite degrees of freedom that arise due to link flexibility. Non-minimum phase nature occurs because of non-collocation of actuators and sensors.

Lets consider, the equations of motion of a flexible link manipulator which can be written in explicit form as

$$M(q)\ddot{q} + C(q,\dot{q})\dot{q} + D\dot{q} + Kq = B\tau \tag{3.1}$$

Where, $q_i = \begin{bmatrix} q_r & q_f \end{bmatrix}^T$ $q = [q_r\ q_f]^T$ are rigid and elastic coordinates of the manipulator; q_r is the $n \times 1$ vector that represents rigid body rotations of the n manipulator joints, and q_f is the $m \times 1$ vector that represent elastic coordinates of the link. The number of elastic coordinates depends on the number of finite elements used to discretize the link. $M(q)$ is the Inertia matrix, $C(q,\dot{q})\dot{q}$ is the Coriolis and centrifugal vector, $D\dot{q}$ is the frictional and damping forces, Kq represents the internal forces due to body elasticity. Input matrix B maps the external torque into generalized forces of the system.

The equations of m otion explicitly written in rigid and elastic coordinates are

$$\begin{bmatrix} M_{rr} & M_{rf} \\ M_{fr} & M_{ff} \end{bmatrix}\begin{bmatrix} \ddot{q}_r \\ \ddot{q}_f \end{bmatrix} + \begin{bmatrix} C_{rr} & C_{rf} \\ C_{fr} & C_{ff} \end{bmatrix}\begin{bmatrix} \dot{q}_r \\ \dot{q}_f \end{bmatrix} + \begin{bmatrix} D_{rr} & 0 \\ 0 & D_{ff} \end{bmatrix}\begin{bmatrix} \dot{q}_r \\ \dot{q}_f \end{bmatrix} + \begin{bmatrix} 0 & 0 \\ 0 & K_{ff} \end{bmatrix}\begin{bmatrix} q_r \\ q_f \end{bmatrix} = \begin{bmatrix} B_r \\ B_f \end{bmatrix}\tau \tag{3.2}$$

The actuators are assumed to be placed at manipulator joints. Thus, the input matrix

B is expressed as $B_r = I_{nXn}$ and $B_f = 0_{mXn}$. The model inversion of equation (3.2), that maps input torque and desired output trajectory, depends on the rigid and elastic coordinates of the system. If the desired output trajectory is the tip trajectory, the system is unstable due to non-minimum phase nature.

The following model based controllers are designed for the trajectory tracking.

– PD Control
– Stable Inversion Control
– A Nonlinear Control
– Adaptive Control

Among them, PD control and Stable inversion control are derived using feedback linearization technique. A nonlinear control and Adaptive control are derived using sliding mode technique.

3.1 PD Control

The control architecture of PD type control is shown in Figure (3.1). It consists of feedforward compensator and a PD feedback loop.

Using equation (3.2), the feedforward compensator is defined as

$$\tau = M_{rr}\ddot{q}_r + M_{rf}\ddot{q}_f + C_{rr}\dot{q}_r + C_{rf}\dot{q}_f + D_{rr}\dot{q}_r \tag{3.3}$$

The coupling effect of rigid body motion and elastic deformations of flexible link in equation (3.3) is ignored to study the effect of flexibility in control design. The equation (3.3) is rewritten as

$$\tau = M_{rr}\ddot{q}_r + C_{rr}\dot{q}_r + D_{rr}\dot{q}_r \tag{3.4}$$

A PD type feedback control at joint space is designed to ensure the stability for unmodeled dynamics. It is written as

$$\tau = M_{rr}(\ddot{q}_r + K_P e_r + K_v \dot{e}_r) + C_{rr}\dot{q}_r + D_{rr}\dot{q}_r \tag{3.5}$$

The control architecture of PD type control is shown in Figure 3.1.

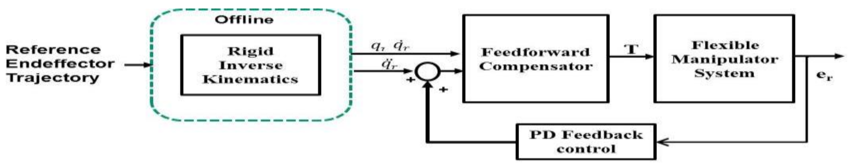

Figure 3.1 - PD control architecture.

The feedforward compensator is shown in Figure 3.2.

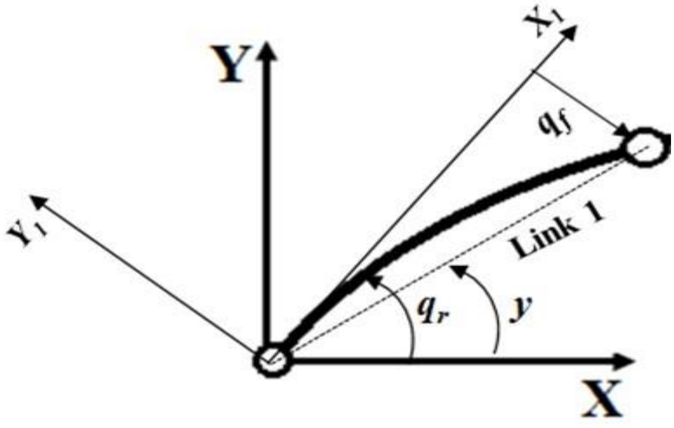

Figure 3.2 - Representation of flexible link tip position at the joint space

Where, K_P and K_v are the position and velocity error gain, respectively; e_r and $\dot{e}_r$ are the joint trajectory error at position and velocity level, respectively.

The equation (3.5), is exactly similar to computed torque control of rigid link manipulator. The objective of this PD control implementation is to analyse the contribution of link flexibility in control design.

3.2 Singular Perturbation Control

The control architecture of stable inversion control is shown in Figure (3.3). It consists of a feedforward compensator and a robust feedback control to achieve desired tip trajectory tracking. Feedforward compensator is derived with the help of stable inversion technique. Stable inversion technique solves the non-minimum phase system by pre-computing bounded internal states q_f for the tip position $y(t)$. The representation of link tip position is shown in Figure 3.2.

Stable inversion control architecture shown in Figure 3.3.

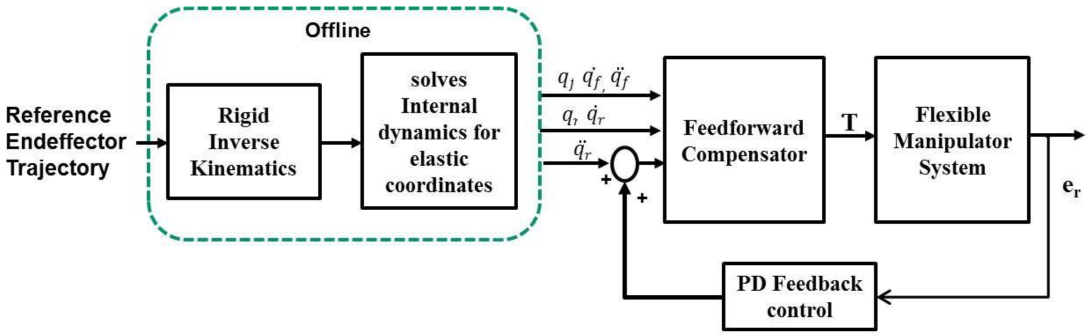

Figure 3.3 - Stable inversion control architecture

The actual tip position is defined as a nonlinear function in terms of joint rotation q_r and elastic coordinates q_f.

$$y = q_r + \arctan\left(\frac{q_f}{L}\right) \tag{3.6}$$

Where y, q_r, and q_f are respectively the tip position, joint angle, and link elastic displacement. To simplify the coupling between tip position and link elastic displacement, the actual tip position is approximated using joint angle and elastic displacement by a weighted parameter. Using weighted parameter, the tip position is redefined as a linear combination of joint angle and link tip elastic coordinates

$$y \approx q_r + \left(\frac{q_f}{L}\right) = q_r + \Gamma q_f \tag{3.7}$$

Where, Γ is the weighted parameter equal to the reciprocal of link length.

In order to compute bounded internal states, the internal dynamics of the system is rewritten in terms of tip position y and elastic coordinates q_f using equation (3.2)

$$M_{fr}(\ddot{y} - \Gamma\ddot{q}_f) + M_{ff}\ddot{q}_f + C_{fr}(\dot{y} - \Gamma\dot{q}_f) + C_{ff}\dot{q}_f + D_{ff}\dot{q}_f + K_{ff}q_f = 0 \tag{3.8}$$

Iterative Learning Method

Internal dynamics of the system is solved using simple PD type Iterative learning method. This method is applied on the nominal dynamic model of the system, since dynamics of the unmodeled payload mass is unknown prior to consider in the dynamic model.

Learning process for the internal dynamics of the system is expressed in terms of deformation torque error,

$$\begin{aligned} e_d(q_f, \dot{q}_f, \ddot{q}_f) = M_{fr}(\ddot{y} - \Gamma\ddot{q}_f) + M_{ff}\ddot{q}_f + C_{fr}(\dot{y} - \Gamma\dot{q}_f) + C_{ff}\dot{q}_f + \\ + D_{ff}\dot{q}_f + K_{ff}q_f \end{aligned} \tag{3.9}$$

The bounded elastic coordinates in time domain for the given reference trajectory $y(t)$ is calculated as follows [8]

1. Set initial values $q_f^{(0)}, \dot{q}_f^{(0)}, \ddot{q}_f^{(0)}$ to zero along the trajectory. Set $i = 0$
2. Using equation (3.9), compute $e_d^{(i)}\ (q_f^{(0)}, \dot{q}_f^{(0)}, \ddot{q}_f^{(0)})$

If $\left\| e_d^{(i)} \right\| < \epsilon_e$, where $_e$ is error tolerance, set $q_{fd} = q_f^{(i)}$ and stop. Else process error using finite impulse response [FIR] filter; $e^{(i)}$ and $\dot{e}^{(i)}$ are thus obtained

3. Update the $q_f^{(i+1)}$ using simple PD type learning rule

$$q_f^{(i+1)} = q_f^{(i)} - K_{LP} e_d^{(i)} - K_{LD} \dot{e}_d^{(i)} \tag{3.10}$$

with small gains K_{LP} and K_{LD}. Set $i = i + 1$ and go to step 2.

Feedforward Compensator

Feed forward compensator is derived using a stable inversion technique. The bounded elastic states q_f, $\dot{q}_f$, $\ddot{q}_f$ are pre-computed using iterative learning method. Thus, the model inversion is stable for the link tip position $y(t)$. The torque required to drive the system along the tip trajectory is computed using

$$\tau = M_{rr}\ddot{q}_r + M_{rf}\ddot{q}_f + C_{rr}\dot{q}_r + C_{rf}\dot{q}_f + D_{rr}\dot{q}_r \tag{3.11}$$

However, the computed torque shown in equation [3.11] works well for the exact model. A simple PD feedback control with arbitrary gains provides accurate trajectory tracking. The closed loop computed torque control is written as

$$\tau = M_{rr}(\ddot{q}_r + K_P e_r + K_v \dot{e}_r) + M_{rf}\ddot{q}_f + C_{rr}\dot{q}_r + C_{rf}\dot{q}_f + D_{rr}\dot{q}_r \tag{3.12}$$

Where, K_P and K_v are the position and velocity error gain, respectively. e_r is the joint trajectory error i.e.

$$e_r = q_{rd} - q_r \tag{3.13}$$

Where q_{rd} is the desired joint trajectory, computed using the bounded elastic coordinates q_f and the tip trajectory $y(t)$ from the Iterative learning method. To account for model uncertainties and unknown payload mass M_p, a robust feedback loop is designed based on conventional rigid manipulator dynamics.

Robust feedback control

Lyapunov function is used to design feedback gains to guarantee the stability along the trajectory with uncertainty in the model. Consider a nominal model

$$\bar{M}\ddot{q} + \bar{C}(q,\dot{q})\dot{q} + \bar{D}(q) = B\tau \tag{3.14}$$

A feedback linearization to a nominal model gives the tracking error dynamics for the joint variable q_r as

$$\begin{bmatrix} \dot{e}_r \\ \ddot{e}_r \end{bmatrix} = \begin{bmatrix} 0 & I \\ 0 & 0 \end{bmatrix} \begin{bmatrix} e_r \\ \dot{e}_r \end{bmatrix} + \begin{bmatrix} 0 \\ I \end{bmatrix} u \tag{3.15}$$

Due to the uncertainties present in $M(q)$ and $C(q, \dot{q})$, the tracking error dynamics have an additional nonlinear term η, which is nonlinear function of both e_r and u.

$$\dot{e}_r = Ae_r + B(u + \eta) \tag{3.16}$$

$$\eta = \Delta(u - \ddot{q}_r) + M^{-1}\delta \tag{3.17}$$

Where,

$$\Delta = M^{-1}\overline{M} - I_n \tag{3.18}$$

And

$$\delta = C - \bar{C} \tag{3.19}$$

To derive the stability conditions the following assumptions are made with finite constants defining the size of uncertainty [7]

$$\frac{1}{\mu_2} \leq \|M^{-1}\| \leq \frac{1}{\mu_1} \tag{3.20}$$

$$\|\Delta\| \leq a \leq 1 \tag{3.21}$$

$$\|\delta\| \leq \beta_0 + \beta_1\|e_r\| + \beta_2\|e_r\|^2 \tag{3.22}$$

$$\|\ddot{q}_{rd}\| \leq c \tag{3.23}$$

Consider a feedback controller

$$u = -Ke_r \tag{3.24}$$

such that

$$\dot{e}_r = Ae_r + B(u + \eta) = (A - BK)e_r + B\eta = A_c + B\eta \tag{3.25}$$

By placing the poles far from the left-half of the plane, the stability of closed loop system in the presence of η is guaranteed. Solving Lyapunov equation

$$A_cP + PA_c = -Q \tag{3.26}$$

with the choice of

$$Q = \begin{matrix} K_p^2 & 0 \\ 0 & 2K_v^2 - 2K_p \end{matrix} \tag{3.27}$$

And

$$K_v^2 > K_p \tag{3.28}$$

the positive definite solution of equation (3.26) is written as

$$P = \begin{matrix} 2K_pK_v & K_p \\ K_p & K_v \end{matrix} \tag{3.29}$$

and feedback gains is defined as

$$K = B^T P = \left[\frac{{K_v}^2}{a} \quad K_v \right] \qquad 3.30)$$

The closed loop system equation (3.25) is uniformly bounded [7] if e_r (0) = 0, $\dot{e}_r$ (0) = 0 and

$$a > 1 + \frac{1}{\mu}\left[\beta_0 + 2(\beta_2\beta_0 + \beta_2(\mu_1 + \mu_2)c)^{\frac{1}{2}}\right]\beta_1 \tag{3.31}$$

Where,

$$K_v = 2aI \tag{3.32}$$

and

$$K_p = 4aI \tag{3.33}$$

Where, K_p and K_v are position and velocity error gains, respectively. I is a $n \times n$ identity matrix. In this way, for the positive K_p and K_v gains the closed loop system is asymptotically stable.

3.3. A Nonlinear Control

The control architecture of a nonlinear control is shown in Figure 3.4.

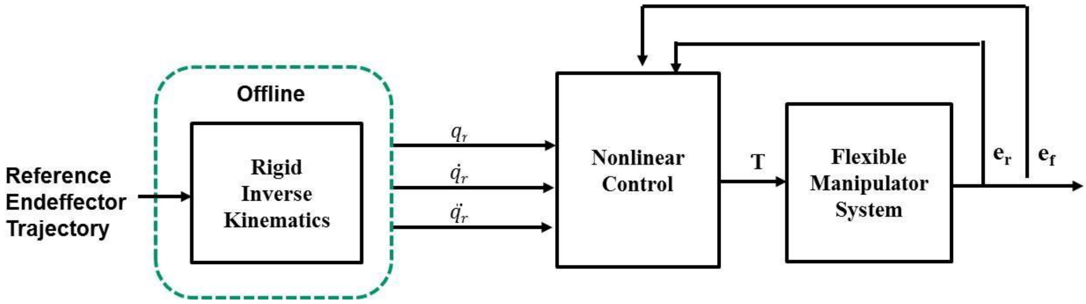

Figure 3.4 - A nonlinear control architecture

3.3 A Nonlinear Control

The control architecture of a nonlinear control is shown in Figure 3.4. The Lyapunov function is used to show the asymptotic stability of closed loop system. Consider the dynamic model

$$M(q)\ddot{q} + C(q,\dot{q})\dot{q} + D\dot{q} + Kq = B\tau \tag{3.34}$$

Position error along the trajectory is defined as

$$e = \begin{bmatrix} e_r \\ e_f \end{bmatrix} = \begin{bmatrix} q_{rd} - q_r \\ q_{fd} - q_f \end{bmatrix} \tag{3.35}$$

Where, q_{rd} and q_{fd} are the desired rigid and flexible coordinates. q_{fd} is set to zero to suppress vibrations.

$$e = \begin{bmatrix} q_{rd} - q_r \\ -q_f \end{bmatrix} \tag{3.36}$$

Lets define the sliding surface s as

$$s = \dot{e} + \lambda\, e = \begin{bmatrix} \dot{e}_r + e_r \lambda_r \\ \dot{e}_f + e_f \lambda_f \end{bmatrix} \tag{3.37}$$

Where,

$$\lambda = \begin{bmatrix} \lambda_r & 0 \\ 0 & \lambda_r \end{bmatrix} \qquad 3.38)$$

The error dynamics of the system with newly defined signal S_r and S_f can be derived as

$$\begin{bmatrix} M_{rr} & M_{rf} \\ M_{fr} & M_{ff} \end{bmatrix} \begin{bmatrix} \dot{s}_r \\ \dot{s}_f \end{bmatrix} + \begin{bmatrix} C_{rr} & C_{rf} \\ C_{fr} & C_{ff} \end{bmatrix} \begin{bmatrix} s_r \\ s_f \end{bmatrix} + \begin{bmatrix} D_{rr} & 0 \\ 0 & D_{ff} \end{bmatrix} \begin{bmatrix} s_r \\ s_f \end{bmatrix} + \begin{bmatrix} 0 & 0 \\ 0 & K_{ff} \end{bmatrix} \begin{bmatrix} s_r \\ s_f \end{bmatrix} = \begin{bmatrix} \tau_m + K_{vr} s_r - \tau \\ \tau_a \end{bmatrix} \tau \tag{3.39}$$

Where,

$$\tau_m = M_{rr}(\ddot{q}_{rd} + \lambda_r \dot{e}_r) + M_{rf}(- \lambda_f \dot{e}_f) + C_{rr}(\dot{q}_{rd} + \lambda_r e_r) + C_{rf}(- \lambda_f e_f) + D_{rr}(\dot{q}_{rd} + \lambda_r e_r) \tag{3.40}$$

$$\tau_a = M_{rr}(\ddot{q}_{rd} + \lambda_r \dot{e}_r) + M_{ff}(- \lambda_f \dot{e}_f) + C_{fr}(\dot{q}_{rd} + \lambda_r e_r) + K_{ff} e_f + K_{vf} s_f \tag{3.41}$$

The following function is considered [7] to analyze the asymptotic stability of error dynamics shown in equation (3.39).

$$\dot{Y} = \begin{cases} 2\left(\sqrt{Ya(t)} + b(t)\right) & Y(t) > 0 \\ 2b(t) & Y(t) = 0 \;\; b(t) > 0 \\ \delta & Y(t) = 0 \;\; b(t) \le 0 \end{cases} \tag{3.42}$$

Where,

$$a(t) = \frac{\|s_r\|^2}{\|s_r\|^2 + \epsilon} (s_f^T \tau_a) \tag{3.43}$$

$$b(t) = \frac{-\epsilon}{\|s_r\|^2 + \epsilon} (s_f^T \tau_a) \tag{3.44}$$

and δ is a small positive constant. The above function $Y(t) \geq 0$ for all $t \geq 0$. Let

$k = \sqrt{Y}$ or $k^2 = Y$, then $k(t)$ can be checked to satisfy differential equation

$$\dot{k} = \frac{1}{k} = \frac{\|s_r\|^2 - \epsilon}{\|s_r\|^2 + \epsilon} \left(s_f^T \tau_a\right), \quad k \neq 0 \tag{3.45}$$

Equation (3.45) is a differential equation to check the variable $Y(t)$ is always positive and $k(t)$ is defined to be its root.

The control law with parameter estimates is chosen as

$$\tau = \tau_m + K_{vr} s_r + \tau_f \tag{3.46}$$

Where,

$$\tau_f = \frac{(1+k)s_r}{\|s_r\|^2 + \epsilon}\left(s_f^T \tau_a\right) \tag{3.47}$$

With this proposed controller the error dynamics of the system is obtained as

$$\begin{bmatrix} M_{rr} & M_{rf} \\ M_{fr} & M_{ff} \end{bmatrix}\begin{bmatrix} \dot{s}_r \\ \dot{s}_f \end{bmatrix} + \begin{bmatrix} C_{rr} & C_{rf} \\ C_{fr} & C_{ff} \end{bmatrix}\begin{bmatrix} s_r \\ s_f \end{bmatrix} + \begin{bmatrix} D_{rr} & 0 \\ 0 & D_{ff} \end{bmatrix}\begin{bmatrix} s_r \\ s_f \end{bmatrix} + \begin{bmatrix} K_{vr} & 0 \\ 0 & K_{vf} \end{bmatrix}\begin{bmatrix} s_r \\ s_f \end{bmatrix} = \begin{bmatrix} -\tau_f \\ \tau_a \end{bmatrix} \tag{3.48}$$

The error dynamics written in compact form is

$$M(\dot{q})s + C(q,\dot{q})s + D_s + K_v s = \begin{bmatrix} -\tau_f \\ \tau_a \end{bmatrix} \tag{3.49}$$

The asymptotic stability of the error dynamics shown in equation [??] is analyzed using Lyapunov function [7]

$$V = \frac{1}{2}s^T M(q)s + \frac{1}{2}Y = \frac{1}{2}s^T M(q)s + \frac{1}{2}k^2 \tag{3.50}$$

The control architecture of adaptive control is shown in Figure 3.5.

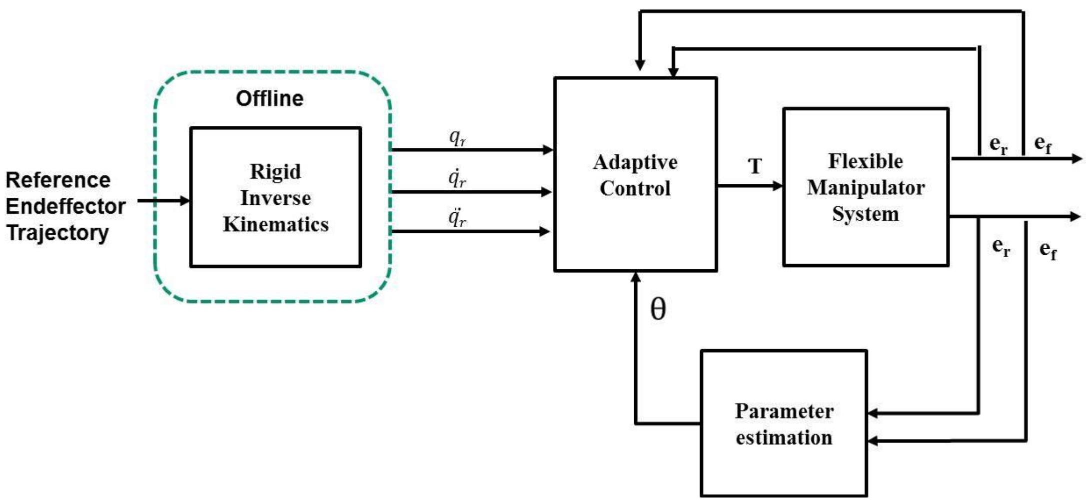

Figure 3.5 - Adaptive control architecture

Differentiating equation (3.50) with respect to time yiel.

$$\dot{V} = \frac{1}{2}s^T M(q)\dot{s} + \frac{1}{2}s^T \dot{M}(q)s + k\dot{k}$$
$$= s^T\left(-Cs - Ds - K_v s + \begin{bmatrix} -\tau_f \\ \tau_a \end{bmatrix}\right) + \frac{1}{2}s^T\dot{M}(q)s$$
$$+ \frac{\|s_r\|^2 - \epsilon}{\|s_r\|^2 + \epsilon}\left(s_f^T \tau_a\right) = -s^T DS - s^T K_v s \quad for\ k > 0 \tag{3.51}$$

Here K_v and D are positive definite, which is clear as $\dot{V} < 0$. Thus, the system is asymptotically stable whenever $k > 0$ and $K_v > 0$.

3.4 Adaptive Control

The control architecture of adaptive control is shown in Figure 3.5. The Lyapunov function is used to show the asymptotic stability of closed loop system.

Consider a nominal model

$$M(q)\ddot{q} + C(q,\dot{q})\dot{q} + D\dot{q} + Kq = B\tau \tag{3.52}$$

Position error along the trajectory is defined as

$$e = \begin{bmatrix} e_r \\ e_f \end{bmatrix} = \begin{bmatrix} q_{rd} - q_r \\ q_{fd} - q_f \end{bmatrix} \tag{3.53}$$

Where, q_{rd} and q_{fd} are the desired rigid and flexible coordinates. q_{fd} is set to zeros to suppress vibrations.

$$e = \begin{bmatrix} q_{rd} - q_r \\ -q_f \end{bmatrix} \tag{3.54}$$

Lets define the sliding surface s as

$$s = \dot{e} + \lambda e = \begin{bmatrix} \dot{e}_r + e_r \lambda_r \\ \dot{e}_f + e_f \lambda_f \end{bmatrix} \tag{3.55}$$

Where,

$$\lambda = \begin{bmatrix} \lambda_r & 0 \\ 0 & \lambda_r \end{bmatrix} \tag{3.56}$$

The error dynamics of the system with newly defined signal S_r and S_f can be derived as

$$\begin{bmatrix} M_{rr} & M_{rf} \\ M_{fr} & M_{ff} \end{bmatrix} \begin{bmatrix} \dot{s}_r \\ \dot{s}_f \end{bmatrix} + \begin{bmatrix} C_{rr} & C_{rf} \\ C_{fr} & C_{ff} \end{bmatrix} \begin{bmatrix} s_r \\ s_f \end{bmatrix} + \begin{bmatrix} D_{rr} & 0 \\ 0 & D_{ff} \end{bmatrix} \begin{bmatrix} s_r \\ s_f \end{bmatrix} + \begin{bmatrix} K_{vr} & 0 \\ 0 & K_{vf} \end{bmatrix} \begin{bmatrix} s_r \\ s_f \end{bmatrix} = \begin{bmatrix} \tau_m + K_{vr} s_r - \tau \\ \tau_a \end{bmatrix} \tag{3.57}$$

Where,

$$\tau_m = M_{rr}(\ddot{q}_{rd} + \lambda_r \dot{e}_r) + M_{rf}(-\lambda_f \dot{e}_f) + C_{rr}(\dot{q}_{rd} + \lambda_r e_r) + C_{rf}(-\lambda_f e_f) + D_{rr}(\dot{q}_{rd} + \lambda_r e_r) \tag{3.58}$$

$$\tau_a = M_{fr}(\ddot{q}_{rd} + \lambda_r \dot{e}_r) + M_{ff}(-\lambda_f \dot{e}_f) + C_{fr}(\dot{q}_{rd} + \lambda_r e_r) + C_{ff}(-\lambda_f e_f) + D_{ff}(-\lambda_f e_f) + K_{ff} e_f + K_{vf} s_f \tag{3.59}$$

The dynamics of the flexible manipulator is expressed in terms of linear type parametric model as

$$W_1 \Theta_1 = M_{rr}(\ddot{q}_{rd} + \lambda_r \dot{e}_r) + M_{rf}(-\lambda_f \dot{e}_f) + C_{rr}(\dot{q}_{rd} + \lambda_r e_r) + C_{rf}(-\lambda_f e_f) + D_{rr}(\dot{q}_{rd} + \lambda_r e_r) \tag{3.60}$$

$$W_2 \Theta_2 = M_{fr}(\ddot{q}_{rd} + \lambda_r \dot{e}_r) + M_{ff}(-\lambda_f \dot{e}_f) + C_{fr}(\dot{q}_{rd} + \lambda_r e_r) + C_{ff}(-\lambda_f e_f) + D_{ff}(-\lambda_f e_f) + K_{ff} e_f + K_{vf} s_f \tag{3.61}$$

Where, W_1 and W_2 are $n \times r_1$, $m \times r_2$ regression matrix for appropriate $r_1, r_2 > 0$; and Θ_1, Θ_2 are unknown constant parameters.

To design adaptive controller for the error dynamics show in equation (3.57), the following function is considered [7]

$$Y = \begin{cases} 2\left(\sqrt{Ya(t) + b(t)}\right) & Y(t) > 0 \\ 2b(t) & Y(t) = 0 \quad b(t) > 0 \\ \delta & Y(t) = 0 \quad b(t) \le 0 \end{cases} \tag{3.62}$$

Where,

$$a(t) = \frac{\|s_r\|^2}{\|s_r\|^2 + \epsilon} (s_f^T W_2 \widehat{\Theta}_2 + s_f^T K_{vf} s_f) \tag{3.63}$$

$$b(t) = \frac{-\epsilon}{\|s_r\|^2 + \epsilon} (s_f^T W_2 \widehat{\Theta}_2 + s_f^T K_{vf} s_f) \tag{3.64}$$

and $\delta\sqrt{}$is a small positive constant. The above function $Y(t) \geq 0$ for all $t \geq 0$. Let $k = Y$ or $k^2 = Y$, then $k(t)$ can be checked to satisfy differential equation

$$\dot{k} = \frac{1}{k} \left(\frac{\|s_r\|^2 - \epsilon}{\|s_r\|^2 + \epsilon} \right) \left(s_f^T W_2 \widehat{\Theta}_2 + s_f^T K_{vf} s_f \right), \quad k \neq 0 \tag{3.65}$$

Equation (3.65) is a differential equation to check the variable $Y(t)$ is always positive and $k(t)$ is defined to be its root.

The control law with parameter estimates is chosen as

$$\tau = W_1 \widehat{\Theta}_1 + K_{vr} s_r + \tau_f \tag{3.66}$$

Where,

$$\tau_f = \frac{(1 + k) s_r}{\|s_r\|^2 + \epsilon} \left(s_f^T W_2 \widehat{\Theta}_2 + s_f^T K_{vf} s_f \right) \tag{3.67}$$

In which, $\widehat{\Theta}_1$ and $\widehat{\Theta}_2$ are the estimates of Θ_1 Θ_2 respectively.

$$\begin{aligned} W_1 \widehat{\Theta}_1 = \widehat{M}_{rr} (\ddot{q}_{rd} + \lambda_r \dot{e}_r) + \widehat{M_{rf}} (- \lambda_f \dot{e}_f) + \hat{C}_{rr} (\dot{q}_{rd} \\ + \lambda_r e_r) + \hat{C}_{rf} (- \lambda_f e_f) + \widehat{D}_{rr} (\dot{q}_{rd} + \lambda_r e_r) \end{aligned} \tag{3.68}$$

$$\begin{aligned} W_2 \widehat{\Theta}_2 = \widehat{M}_{fr} (\ddot{q}_{rd} + \lambda_r \dot{e}_r) + \widehat{M}_{ff} (- \lambda_f \dot{e}_f) + \hat{C}_{fr} (\dot{q}_{rd} + \lambda_r e_r) \\ + \hat{C}_{ff} (- \lambda_f e_f) + \widehat{D}_{ff} (- \lambda_f e_f) + \widehat{K}_{ff} e_f \end{aligned} \tag{3.69}$$

With this proposed controller the error dynamics of the system is obtained as

$$\begin{aligned} \begin{bmatrix} M_{rr} & M_{rf} \\ M_{fr} & M_{ff} \end{bmatrix} \begin{bmatrix} \dot{s}_r \\ \dot{s}_f \end{bmatrix} + \begin{bmatrix} C_{rr} & C_{rf} \\ C_{fr} & C_{ff} \end{bmatrix} \begin{bmatrix} s_r \\ s_f \end{bmatrix} + \begin{bmatrix} D_{rr} & 0 \\ 0 & D_{ff} \end{bmatrix} \begin{bmatrix} s_r \\ s_f \end{bmatrix} + \begin{bmatrix} K_{vr} & 0 \\ 0 & K_{vf} \end{bmatrix} \begin{bmatrix} s_r \\ s_f \end{bmatrix} \\ = \begin{bmatrix} W_1 \widetilde{\Theta}_1 - \tau_f \\ W_2 \widetilde{\Theta}_2 \end{bmatrix} \end{aligned} \tag{3.70}$$

The error dynamics written in compact form is

$$M(q)\dot{s} + C(q, \dot{q})s + Ds + K_{vs} = \begin{bmatrix} W_1 \widetilde{\Theta}_1 - \tau_f \\ W_2 \widetilde{\Theta}_2 \end{bmatrix} \tag{3.71}$$

Where, $\widetilde{\Theta}_1 = \Theta_1 - \widehat{\Theta}_1$ and $\widetilde{\Theta}_2 = \Theta_2 - \widehat{\Theta}_2$ are the parameter estimation error.
The adaptation law is derived as

$$\dot{\widehat{\Theta}}_1 = -K_1 W_1^T s_r \tag{3.72}$$

$$\dot{\widehat{\Theta}}_2 = -K_2 W_2^T s_f \tag{3.73}$$

Where, K_1, K_2 are positive definite matrices. The asymptotic stability of the error dynamics is derived using Lyapunov function

$$\begin{aligned} V &= \frac{1}{2} s^T M(q) s + \frac{1}{2} \widetilde{\Theta}_1^T \mathrm{K}_1^{-1} \widetilde{\Theta}_1 + \frac{1}{2} \widetilde{\Theta}_2^T \mathrm{K}_2^{-1} \widetilde{\Theta}_2 + \frac{1}{2} Y \\ &= \frac{1}{2} s^T M(q) s + \frac{1}{2} \widetilde{\Theta}_1^T \mathrm{K}_1^{-1} \widetilde{\Theta}_1 + \frac{1}{2} \widetilde{\Theta}_2^T \mathrm{K}_2^{-1} \widetilde{\Theta}_2 + \frac{1}{2} k^2 \end{aligned} \tag{3.74}$$

Differentiating equation (3.74) with respect to time yields

$$\begin{aligned} \dot{V} &= s^T M(q) \dot{s} + s^T M(q) \dot{s} + \frac{1}{2} s^T \dot{M}(q) s + \dot{\widetilde{\Theta}}_1^T \mathrm{K}_1^{-1} \widetilde{\Theta}_1 + \dot{\widetilde{\Theta}}_2^T \mathrm{K}_2^{-1} \widetilde{\Theta}_2 + k\dot{k} \\ &= s^T \left(-Cs - Ds - K_v s + \begin{bmatrix} W_1 \widetilde{\Theta}_1 - \tau_f \\ W_2 \widetilde{\Theta}_2 \end{bmatrix} \right) + \frac{1}{2} s^T \dot{M}(q) s \\ &\quad - s_r^T W_1 \widehat{\Theta}_1 - s_f^T W_2 \widehat{\Theta}_2 + \left(\frac{k \|s_r\|^2 - \epsilon}{\|s_r\|^2 + \epsilon} \right) \left(s_f^T W_2 \widehat{\Theta}_2 + s_f^T K_{vf} s_f \right) \\ &= -s^T DS - s^T K_v s + \left(\frac{k \|s_r\|^2 - \epsilon}{\|s_r\|^2 + \epsilon} \right) (s_f^T W_2 \widehat{\Theta}_2 \\ &\quad - \left(\frac{(1+k) \|s_r\|^2 - \|s_r\|^2 - \epsilon}{\|s_r\|^2 + \epsilon} \right) \left(s_f^T W_2 \widehat{\theta}_2 + s_f^T K_{vf} s_f \right) \\ &\quad + s_f^T W_2 \widehat{\theta}_2 - s_f^T W_2 \widehat{\Theta}_2 = -\mathrm{s^T DS} - \mathrm{s^T K_v s} \quad \text{for } \mathrm{k} > 0 \end{aligned} \tag{3.75}$$

Here $\mathrm{K_v}$ and D are positive definite, which is clear as $\dot{V} < 0$. Thus, the system is asymptotically stable whenever $k > 0$ and $\mathrm{K_v} > 0$.

3.5 Simulation Results

A spatial RRR manipulator shown in Figure 3.6, is considered to demonstrate the performance of model based controllers. The manipulator have three flexible links and three rigid revolute joints. Each flexible link is discretized using two finite element beams with six degrees of freedom on each node and one degree of freedom for rigid body rotations i.e. θ_i where i = 1,2,3. The damping effects on links and joints are ignored. The physical parameters of a RRR spatial manipulator are presented in Table 4.1. Uniform cross-section and material properties are assumed on each link.

Table 3.1 - The physical parameters of a RRR flexible manipulator

Parameter	Link 1	Link 2	Link 3
Link Length (m)	1	4.0	3.5
C/s Area (m^2)	0.028	0.0020	0.0008
Moment of Inertia (m^4)	8.33×10^{-7}	6.24×10^{-7}	5.37×10^{-7}
Polar moment of Inertia (m^4)	1.66×10^{-6}	1.24×10^{-6}	1.07×10^{-6}
Density (Kg/m^3)	Tensile Modulus (MPa) 206000 Shear Modulus (MPa) 79300	8253	

The reference trajectories of joint 1, joint 2, and joint 3 are shown in Figure 3.7. The simulation results of PD controller, Stable inversion controller, nonlinear controller, and Adaptive controller are compared. Figure 3.8, Figure 3.9, and Figure 3.10 show the error along joint trajectory θ_1, θ_1, and θ_1 respectively. Figure 3.11,

A spatial RRR manipulator shown in Figure 3.6.

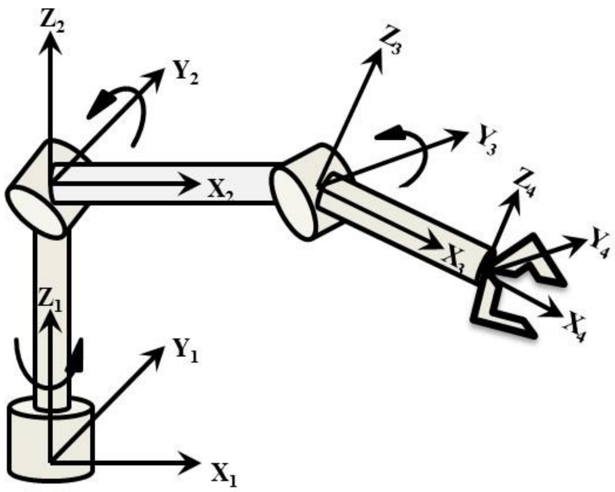

Figure 3.6 - Spatial RRR flexible manipulator with three flexible links and three rigid joints

Reference trajectory shown in Figure 3.7.

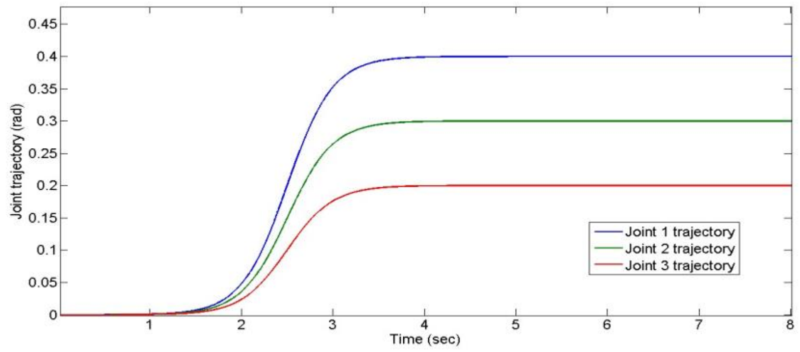

Figure 3.7 - Reference trajectory

Error along joint θ_1 trajectory shown in Figure 3.8.

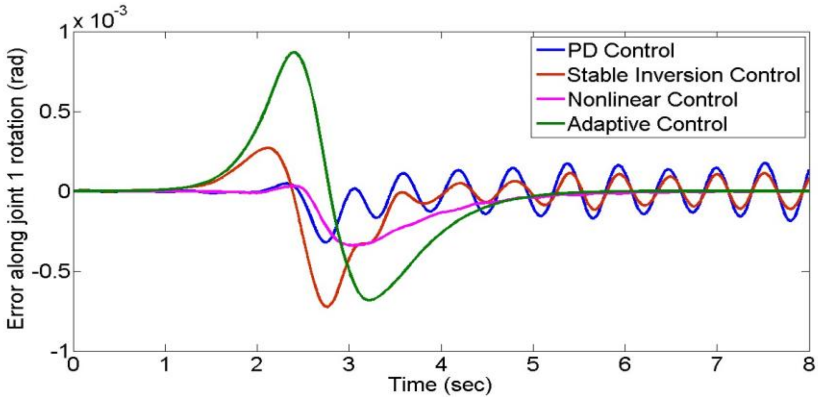

Figure 3.8 - Error along joint θ_1 trajectory

Error along joint θ_2 trajectory shown in Figure 3.9.

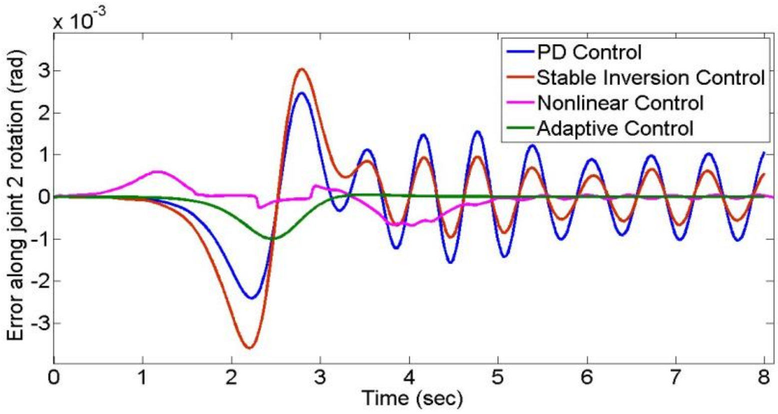

Figure 3.9 - Error along joint θ_2 trajectory

Error along joint θ_3 trajectory shown in Figure 3.10.

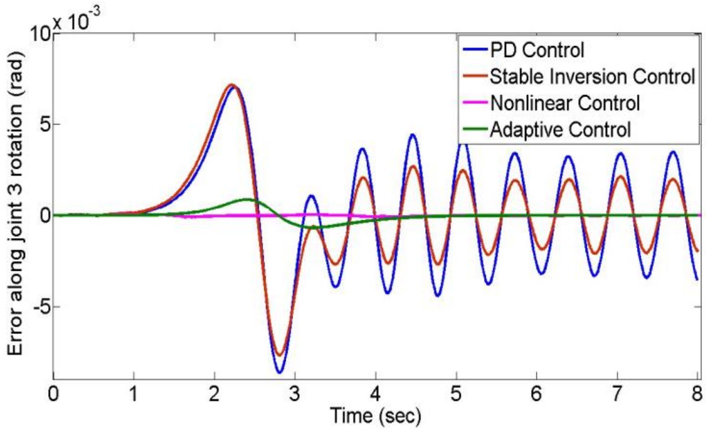

Figure 3.10 - Error along joint θ_3 trajectory

Elastic displacements of endeffector $X_4Y_4Z_4$ along X-Direction shown in Figure 3.10.

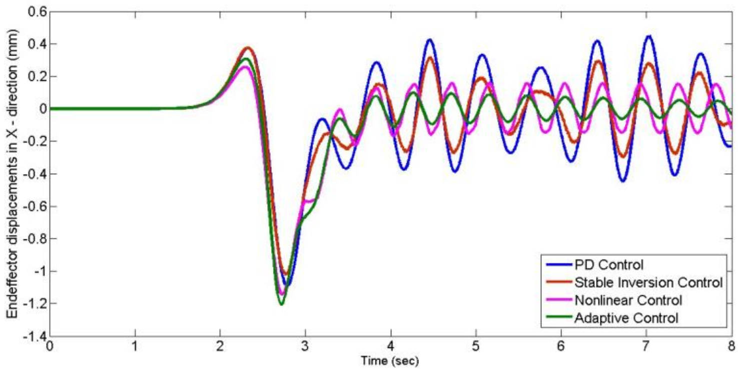

Figure 3.11 - Elastic displacements of endeffector $X_4Y_4Z_4$ along X-Direction

Elastic displacements of endeffector $X_4Y_4Z_4$ along Y-Direction shown in Figure 3.12.

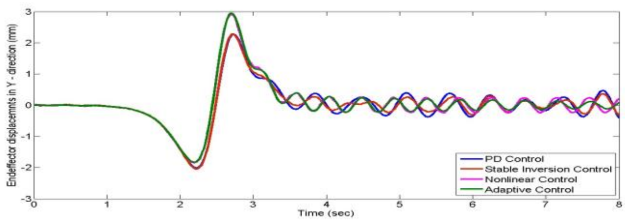

Figure 3.12 - Elastic displacements of endeffector $X_4Y_4Z_4$ along Y-Direction

Elastic displacements of endeffector $X_4Y_4Z_4$ along Z-Direction shown in Figure 3.13.

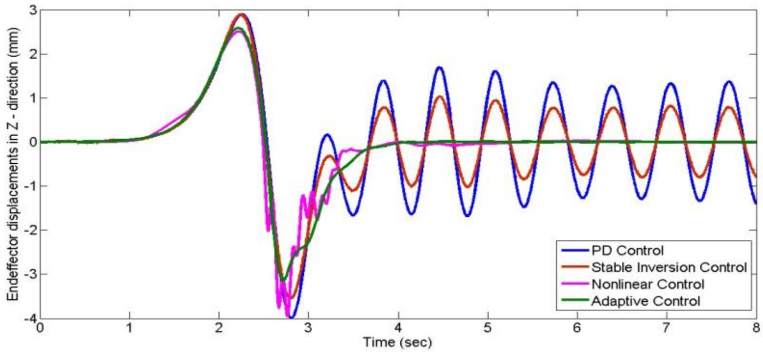

Figure 3.13 - Elastic displacements of endeffector $X_4Y_4Z_4$ along Z-Direction

Figure 3.12, and Figure 3.13 show the endeffector $X_4Y_4Z_4$ elastic displacements along X, Y, and Z direction respectively.

The PD controller is designed based on rigid link manipulator dynamics to study the effect of link flexibility in control design. Thus, the simulation results of PD controller showed good trajectory tracking at joint space but it is not very efficient to damp the endeffector vibrations. It can be seen in Figure 3.11 - 3.13.

The stable inversion control showed better trajectory tracking compared to PD control, however this method is incapable of damping the vibrations in case of unmodeled dynamics such as unknown payload mass. Moreover, stable inversion control have good performance for planar flexible link manipulators compared to spatial flexible link manipulators. These results are shown in chapter [4].

Nonlinear control and adaptive control showed good trajectory tracking at the joint space and also efficient to damp the endeffector $X_4Y_4Z_4$ vibrations compared to PD controller and stable inversion control as it can be seen in Figure 3.11 - Figure 3.13. The endeffector vibrations along Z-direction is damped quickly where as the endeffector vibrations along X-direction and Y-direction are taking long time to damp the vibrations because these vibrations are out-of-plane with respect to actuators at the manipulator joints. To improve the damping properties of the out-of-plane bending vibration additional control effort is required along this direction.

Overall, the adaptive control showed better performance compared to PD controller, stable inversion control and nonlinear control.

4 Experimental results

4.1 Introduction

A single link flexible manipulator shown in Figure 4.1 is designed to demonstrate the performance of the model based controllers that are developed for the trajectory tracking. The experimental setup consists of Quanser SRV02 rotary servo plant, Quanser Q8 terminal board, universal power module (UPM), single link flexible manipulator, and a strain guage. The schematic layout of experimental setup is shown in Figure 4.3.

A strain gauge is mounted close to clamped end of flexible link to measure tip displacements. It is shown in Figure 4.2. The physical parameters of single link manipulator are presented in Table 4.1.

The Quanser SRV02 rotary servo plant consists of actuator and external load gear. The actuator consists of DC motor equipped with internal planetary gearbox. The internal planetary gearbox is connected to external load gear. The assembly of DC motors, internal planetary gear box and external load gear introduce friction and damping at the joint.

The friction model and damping properties are identified using experimental method. The coulomb and viscous Friction model is considered to accurately model the friction behaviour at the joint. The offset value and gain for friction model are computed based on series of experiments by measuring constant angular velocities for given input voltage.

4.2 Model Validation

Lets consider the equations of motion of a flexible link manipulator shown in Figure 4.1.

Figure 4.1- Experimental setup of a single link flexible manipulator

Table 4.1 - The physical parameters of single link planar manipulator

Parameter Name	Nominal Value
Motor Inertia (I_m)	2.08e-3 Kgm^2
Motor Viscous Damping (B_m)	4e-3 $Nm/(rad/s)$
Payload Mass (M_p)	0.1 kg
Dimension of Link (LxHxW)	0.52x0.045x0.002 m
Tensile Modulus	206000 MPa
Density (ρ)	8253 Kg/m^3

$$\begin{bmatrix} M_{rr} & M_{rf} \\ M_{fr} & M_{ff} \end{bmatrix} \begin{bmatrix} \ddot{q}_r \\ \ddot{q}_f \end{bmatrix} + \begin{bmatrix} C_{rr} & C_{rf} \\ C_{fr} & C_{ff} \end{bmatrix} \begin{bmatrix} \dot{q}_r \\ \dot{q}_f \end{bmatrix} + \begin{bmatrix} D_{rr} & 0 \\ 0 & D_{ff} \end{bmatrix} \begin{bmatrix} \dot{q}_r \\ \dot{q}_f \end{bmatrix} + \begin{bmatrix} 0 & 0 \\ 0 & K_{ff} \end{bmatrix} \begin{bmatrix} q_r \\ q_f \end{bmatrix} = \begin{bmatrix} B_r \\ B_f \end{bmatrix} \tau \tag{4.1}$$

Where, q_r and q_f are the rigid and elastic coordinates.

Using the equation [4.1] the feedforward compensator is defined as

$$\tau = M_{rr}\ddot{q}_r + M_{rf}\ddot{q}_f + C_{rr}\dot{q}_r + C_{rf}\dot{q}_f + D_{rr}\dot{q}_r \tag{4.2}$$

For the given reference trajectories q_r, $\dot{q}_r$ and $\ddot{q}_r$, the input torque applied at manipulator joint can be computed by equation (4.2). The values of elastic coordinates q_f, $\dot{q}_f$ and $\ddot{q}_f$ is set to zero because these values are not known apriori.

The out response of the feedforward compensator is shown in Figure 4.2.

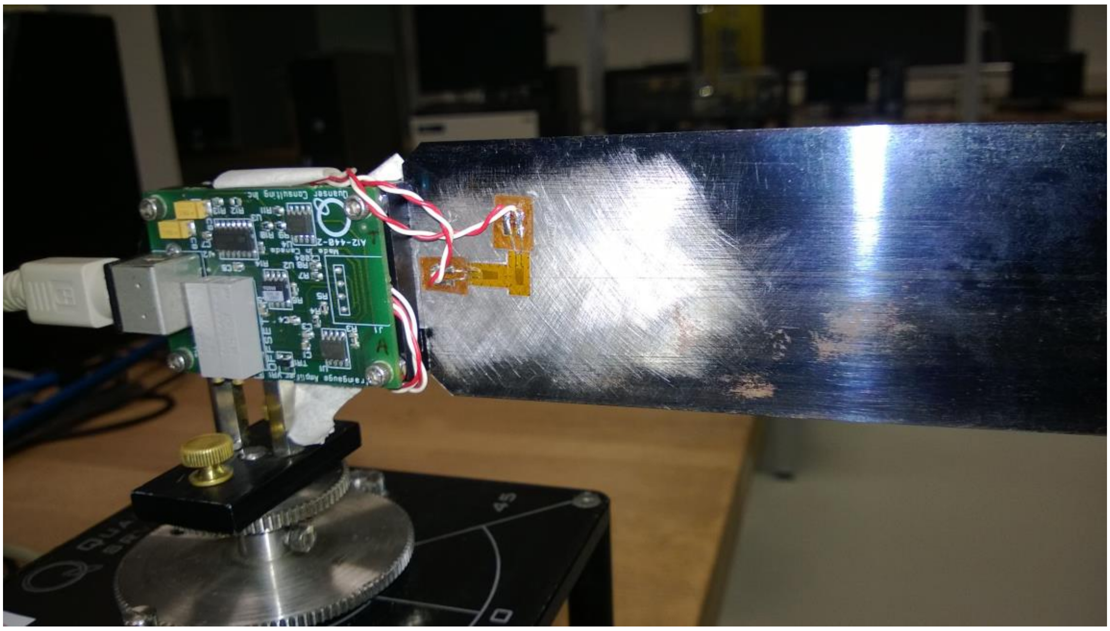

Figure 4.2 - Strain guage mounted on flexible manipulator

Experimental setup of a single link flexible manipulator is shown in Figure 4.3.

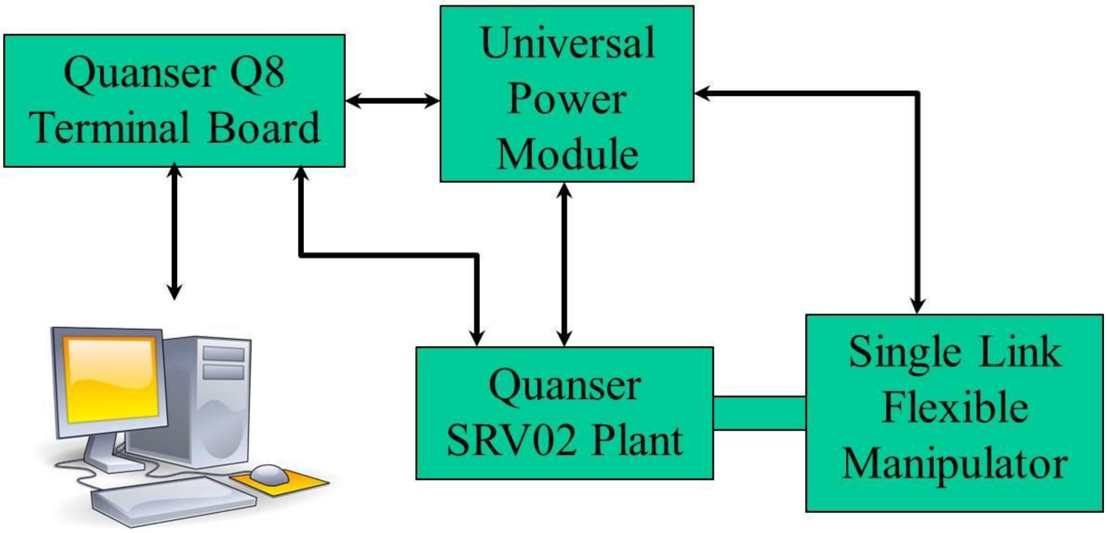

Figure 4.3 - Experimental setup of a single link flexible manipulator

4.3 Friction Compensator

The friction at the manipulator joint plays a major role in the position control. The friction model can be identified using the Newtons first law of motion. The equations of motion of a Qunaser servo plant is defined as

$$T_m(t) - T_f = J_m \dot{\omega}(t) \tag{4.3}$$

Where, T_m is the motor torque, and T_f is the friction torque. J_m is the motor inertia, and $\omega(t)$ is the angular velocity at the load shaft.

From equation (4.3), if the angular velocity is constant then friction torque is equal to motor torque i.e.

$$T_m(t) = T_f \tag{4.4}$$

The torque applied by the servo motor at the manipulator joint can be defined as

$$T_m(t) = \frac{\eta_q k_q \eta_m k_t (V_m - k_g k_m \dot{\theta})}{R_m} \tag{4.5}$$

Where, V_m is the input voltage and $\dot{\theta}$ is the angular velocity of load shaft. The Quanser servo plant parameters are listed in Table [4.2]

Table 4.2 - *Quanser servo plant parameters.*

Parameter	Description	Value

Table continuation 4.2

κ_t	Motor torque constant	7.68E-3 Nm
ηm	Motor efficiency	0.69
κ_g	Total gearbox ratio	70
η_g	Gearbox efficiency	0.90
κm	Back-emf constant	7.68E-3V/(rad/s)
R_m	Motor armature resistance	2.6 Ω

From the equation [4.3] the friction torque is equal to motor torque when the angular velocity is constant. Hence, the frictional torque can be computed using equation (4.5). The angular velocity $\dot{\theta}$ is measured at different constant angular velocities by increasing the input voltage V_m. The measured angular velocity for the given input voltage is shown in Table 4.3.

Table 4.3 - The experimental data: angular velocity measurement vs input voltage.

Voltage	Angular velocity	Motor torque
(volts)	(rad/s)	(Nm)
0.0	0	0
0.1	0	0.0128
0.2	0.095	0.0257
0.3	0.171	0.0385
0.4	0.253	0.0514
0.5	0.331	0.0642
1.0	0.756	0.1284
1.5	1.182	0.1926
2.0	1.614	0.2568

The coulomb and viscous friction model is considered to fit the measured data.

$$F_f(\dot{\theta}) = F_c sgn(\dot{\theta}) + \beta\dot{\theta} \tag{4.6}$$

Where, F_f is the total frictional torque, F_c is the coulomb friction torque, β is theviscous friction coefficient and $\dot{\theta}$ is the angular velocity.

From Table 4.3 the motor begins to rotate between the input voltage 0.1 V and 0.2 V. To find out the precise value of input voltage where the motor begins to rotate, the angular velocity $\dot{\theta}$ is measured for very small increments of voltage. It is noticed that at input voltage 0.11 V the motor begins to rotate. Thus the coulomb friction torque is defined as this point.

The coulomb frictional torque value is computed as

$$F_c = 0.0141Nm \tag{4.7}$$

The viscous friction coefficient β is computed using the slope of frictional torque plotted in Figure 4.4. It is defined as

$$\beta = \frac{change\ in\ the\ friction\ torque}{change\ in\ the\ angular\ velocity} = 0.1496 \tag{4.8}$$

The viscous friction coefficient β is computed using the slope of frictional torque plotted in Figure 4.4.

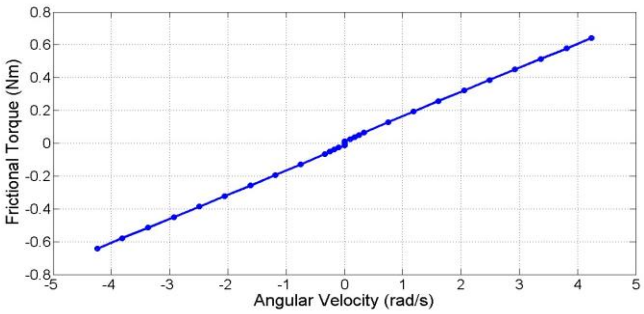

Figure 4.4 - Frictional torque F_f vs angular velocity plot using experimental data

4.4 Experimental Results

The following model based controllers are experimentally verified on single link flexible manipulator.

1. PD Control
2. Stable Inversion Control
3. Adaptive Control

The joint trajectory response of open loop system is shown in Figure 4.5.

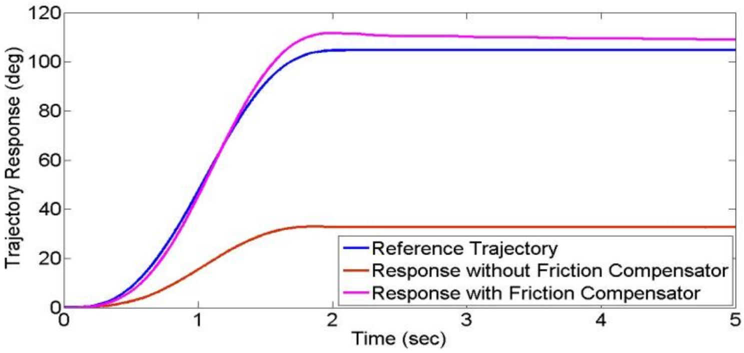

Figure 4.5 - The joint trajectory response of open loop system

The joint trajectory response is shown in Figure 4.6.

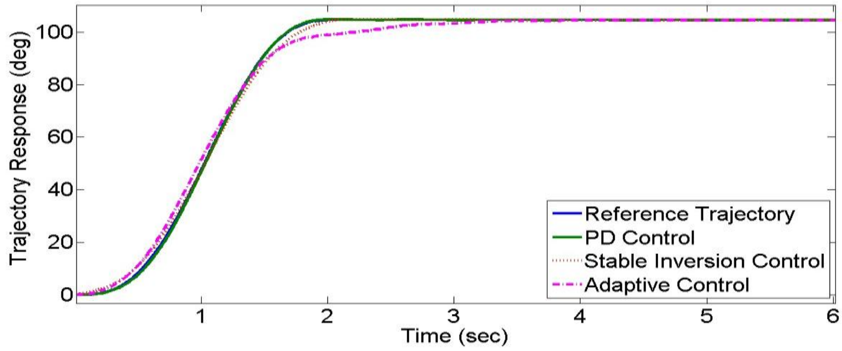

Figure 4.6 - The joint trajectory response

The performance of the model based controllers are tested in the presence of addition payload mass on the tip.

Figure 4.6 show the comparison between PD controller, stable inversion controller, and adaptive controller without payload mass. Figure 4.7 show the trajectory tracking error. Figure 4.8 show the tip displacements along the trajectory.

Figure 4.9 show the comparison between PD controller, stable inversion controller, and adaptive controller in the presence of additional payload mass. Figure 4.10 show the trajectory tracking error. Figure 4.11 show the tip displacements along the trajectory.

The experimental results show that stable inversion controller and adaptive controller have accurate trajectory tracking without payload mass on tip. In the presence of additional payload mass $M_p = 0.1$ Kg, adaptive control showed better tip trajectory tracking compared to PD controller, and stable inversion controller.

Trajectory tracking error is shown in Figure 4.7.

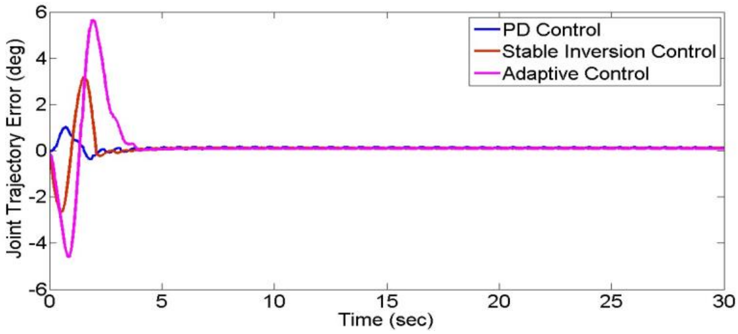

Figure 4.7 - The error along joint trajectory

Tip displacement along the trajectory is shown in Figure 4.8.

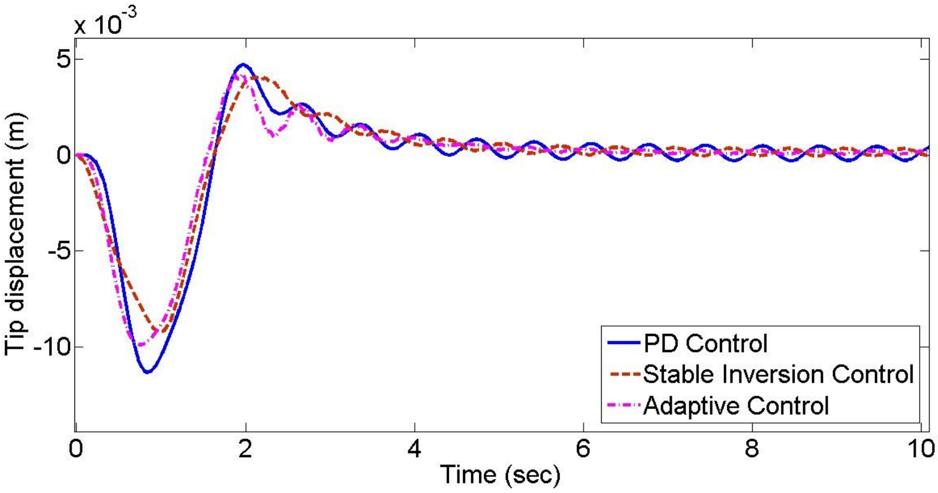

Figure 4.8 - Tip displacement along the trajectory

The advantage of the stable inversion control is that it does not require measurement of the tip displacement because these values are estimated off-line using Iterative learning method. The stable inversion control showed good trajectory tracking and minimized vibrations without payload mass as it is seen in Figure 4.7 and Figure 4.8, but for additional payload mass the stable inversion control is not efficient to damp the vibrations because the estimated off-line elastic displacements heavily depend on the accuracy of the dynamic model which is unknown a priori in case of unknown payload mass.

The adaptive control measures tip displacement along the trajectory and minimizes the tip vibrations. It has tip displacements and joint trajectory error as a feedback in the control. Thus, adaptive control showed better performance in trajectory tracking and vibration suppression in the presence of additional payload mass.

Figure 4.9 show the comparison between PD controller, stable inversion controller, and adaptive controller in the presence of additional payload mass.

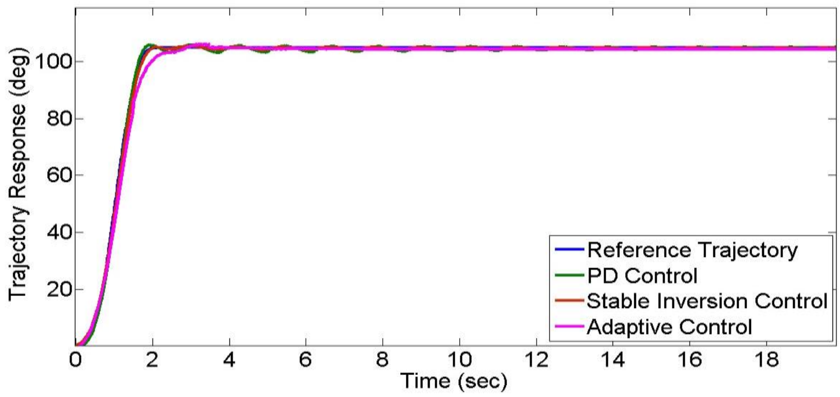

Figure 4.9 - The joint trajectory response in the presence of additional payload mass

Figure 4.10 show the trajectory tracking error.

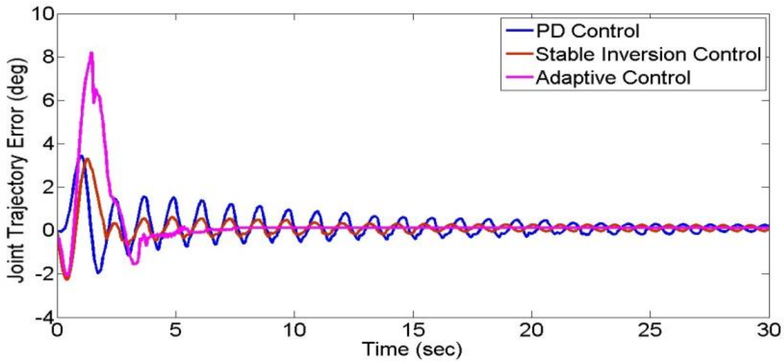

Figure 4.10 - The error along joint trajectory in the presence of additional payload mass

Figure 4.11 show the tip displacements along the trajectory.

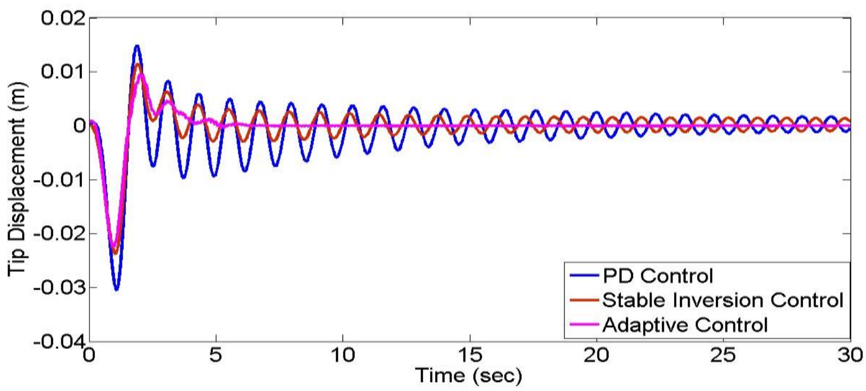

Figure 4.11 - Tip displacement along the trajectory in the presence of additional payload mass

5 Life safety

5.1 To determine the category of labor severity through an integrated ball score

The working environment of a human operator is a combination of physical, chemical, biological, socio-psychological and aesthetic environmental factors affecting the operator [1 - 5].

The severity of labor is a characteristic of labor activity, which is determined by the degree of the cumulative effect of the production elements of working conditions on the functional state of the human body, its working capacity, ability to work, health, the process of reproduction of labor and labor efficiency. Different reactions and various changes that occur in the body under the influence of specific working conditions at the workplace are the basis for determining the category of labor severity.

There are four levels of the impact of working environment factors on humans, necessary for their accounting and rationing [1]:

1. a comfortable environment provides optimal dynamics of the operator’s working ability, well-being and preservation of his health;
2. the relatively uncomfortable working environment provides, when exposed for a certain period of time, a given working ability and maintaining health, but it causes subjective sensations and functional changes in a person that do not go beyond the norm;
3. extreme working environment leads to a decrease in the operator’s working capacity and causes functional changes that go beyond the norm, but do not lead to pathological changes or the inability to perform work;
4. superextreme environment leads to the occurrence of pathological changes in the human body or the inability to perform work.

A comprehensive assessment of the working environment factors is carried out based on the methodology of physiological classification of the severity of work [1, 5]. Thus, the work performed by gravity is divided into six categories of labor severity.

The first category (I) includes work performed under optimal conditions of the working environment with favorable physical, mental and neuro-emotional stress.

The second category (II) includes work carried out under conditions in which the actual levels of production factors correspond to the maximum permissible concentrations according to the current sanitary rules, norms and hygienic standards.

The third category (III) includes work in which, due to not quite favorable working conditions, the worker forms reactions that are characteristic of the borderline state of the body. At the same time, some physiological functions during work can deteriorate, especially towards the end of the working day as compared to the standard level, which leads to a decrease in production indicators.

The fourth category (IV) includes work in which the impact of adverse (dangerous and harmful) production factors leads to reactions characteristic of a deeper (pre-pathological) borderline state in practically healthy people. The majority of physiological indicators in this case worsens, especially at the end of working periods; performance and attention are supported only by mobilizing additional resources (reserves) of the body.

The fifth category (V) includes work in which, as a result of exposure to very unfavorable working conditions, workers at the end of the working period (shift, week) form reactions characteristic of the pathological state of the body in practically healthy people who do not have medical contraindications to such work. This is especially noticeable with high neuro-emotional stress. Performance indicators sharply worsen, occupational diseases are possible.

The sixth category (VI) includes work in which such reactions occur shortly after the start of the labor period. A high level of occupational morbidity is possible, the level of occupational injuries is increasing.

Quantitative analysis of the severity and intensity of labor

Working conditions have a direct impact on the state of the body, which is characterized by certain reactions. To assess the negative impact on a person of external conditions, it is necessary to determine the category of severity of work.

When conducting a quantitative analysis of the severity of labor, sanitary-hygienic and psychophysiological factors of the working environment that characterize working conditions should be taken into account.

In accordance with GOST, the sanitary-hygienic factors of the working environment should include:

- microclimate in the working area;
- the presence and concentration of harmful substances of various hazard classes;
- the presence and concentration of industrial dust;
- vibroacoustic factors and ultrasound;
- the intensity of thermal radiation;
- electromagnetic radiation of various frequency ranges; - ionizing radiation (x-ray, gamma, α-β radiation);
- biological factors.
- According to GOST, psychophysiological factors include:
- physical, dynamic and static loads;
- working pose and moving in space;
- shift, duration of continuous work during the day;
- category of visual work;
- the number of important objects of observation;
- pace of work, monotony of work;
- the amount of information received and processed;
- mode of work and rest;
- neuro-emotional stress;
- intellectual load.

- According to GOST, psychophysiological factors include:
- physical, dynamic and static loads;
- working pose and moving in space;
- shift, duration of continuous work during the day;
- category of visual work;
- the number of important objects of observation;
- pace of work, monotony of work;
- the amount of information received and processed;
- mode of work and rest;
- neuro-emotional stress;
- intellectual load.

When conducting the analysis, factors of the working environment that are characteristic of a given workplace and a particular profession are taken into account. As a rule, working conditions are determined by a combination of factors of the working environment, therefore, each indicator or environmental factor must be rated in points from 1 to 6 depending on their numerical value (Appendix 1, tables 1.1-1.3).

The category of severity and intensity of work is directly related to the integral point estimate, which can be determined by the formula:

$$u_r = \left[x_{max} + \frac{\sum_{i=1}^{n} x_i}{n-1} \times \frac{6 - x_{max}}{6}\right] \times 10, \quad (5.1)$$

Where, x_{max}- the largest of the private scores received ratings; x_i - score on the i-th of the factors taken into account; n is the total number of factors excluding one factor Xmax; N is the total number of factors.

The dependence of the severity category on the integrated scoring is given in table 1.

Table 5.1 - Categories of severity of labor

Labor severity category	1	2	3	4	5	6
Integral assessment of elements of working conditions, UT, points	before 18	18,1-33	33,1-45	45,1-53	53,1-59	59,1-60

If the harmful factor does not affect during the entire shift, then the assessment of factors and indicators of working conditions should be determined depending on the time of their exposure to the employee:

$$\mathrm{x}_{i\,fac} = \mathrm{x}_i \frac{t}{t_{cm}} \quad (5.2)$$

Where, x_i - assessment of the i-th element of working conditions in points;
t - the actual duration of the factor, min. ;
t_{cm} - shift duration, min.

An increase in the severity of labor will affect a person's performance. The decrease in working capacity is directly related to the state of fatigue, which can be quantified using the fatigue index expressed in arbitrary units. The relationship between the integral indicator of the severity of labor and the degree of fatigue can be expressed by the equation:

$$Y = \frac{U_r - 15{,}6}{0{,}64} \tag{5.3}$$

Where, y -an indicator of fatigue in arbitrary units;
15.6 and 0.64 are regression coefficients;
U_r is an integral indicator of the category of labor severity in points.

If you know the degree of fatigue, then you can determine the level of performance by the formula

$$R=100- Y, \tag{5.4}$$

Where, R is the level of performance in relative units.

According to the values of performance determined before and after measures to improve working conditions, you can calculate the change in labor productivity (productivity increase) by the formula:

$$\Pi_{nm} = \left[\frac{R_2}{R_1} - 1\right] \times 100 \times 0{,}2\ , \tag{5.5}$$

Where, Π_{nm} is the increase in labor productivity;
R_2 and R_1 - performance in arbitrary units before and after measures to improve and improve working conditions;
0,2 - correction factor, which reflects the relationship between an increase in working capacity and an increase in labor productivity.

The severity and intensity of work has an impact on the growth of occupational injuries. Since the integral point assessment makes it possible to determine the category of labor severity, the value of occupational injuries can be calculated by the formula:

$$K = \frac{1}{1{,}3 - 0{,}0185 \cdot U_T} \tag{5.6}$$

Where, K is the growth of industrial injuries, the number of times; U_T is an integral indicator of the category of labor severity in points.

In the workplace, provision should be made for the creation of a favorable working environment and the formation of working conditions that will fall into the first category of work severity (optimal). If the equipment has a low risk of injury and high productivity, then the value of injuries can be taken equal to unity, and in this case, the integral indicator of the severity of labor will be equal to:

$$U_T = (1{,}3\text{-}1{,}0) \,/\, 0{,}0185 = 16{,}2 \qquad (5.7)$$

what will characterize the best safety of the given workplace.

Required:

As a result of measures for safety and labor protection, indicators of factors of the working environment and working conditions have changed. To determine the dynamics of changes in industrial injuries and working capacity for a particular workplace, as well as an increase in labor productivity.

Table 5.2

Profession	Working environment factor and working conditions	Value indicator before moderni-zation	Value indicator before moderni-zation	Duration of action
Operator automation world	RM air temperature in the warm season, C^0	33	20	480
	Exceeding Sound Level, дБа	98	90	480/42 0
	RM stationary, free pose	--		480
	The mass of transported goods	until 5 kg	until 2 kg	480
	Morning shift work	-	-	-
	Duration of continuous work during the day, hours	8	6	480
	Duration of concentrated observation,% of the duration of the work shift	80	60	480/24 0
	Reasonable mode of work and rest using functional music and gymnastics	-	-	-
	Neuro-emotional stress arises as a result of simple actions according to an individual plan	-	-	-

Based on the source data and tables of Appendix 1, we place points for each factor in the working environment and the indicator before and after measures to improve working conditions. When assessing, it is necessary to adjust the value of the score depending on the exposure time. The evaluation results are presented in table form table 5.3.

Table 5.3

Working environment factor and working conditions	Indicator value	Score factors	
		Before events	After events
RM air temperature in the warm season, C^0	10/20	5	1
Exceeding Sound Level, дБа	98/90	4	3
RM stationary, free pose, the mass of transported goods	6/2	2	1
Morning shift work Duration of continuous work during the day, hours	8/6	1	1
Duration of concentrated observation,% of the duration of the work shift	80/60	3	2
Reasonable mode of work and rest using functional music and gymnastics		4	3
Neuro-emotional stress arises as a result of simple actions according to an individual plan		1	1

After scoring factors and indicators, I calculated the integral assessment of the severity of labor before and after the events according to the formula:

a) before measures to improve working conditions:

$$U_1 = \left[5 + \frac{4+2+3+4+1+1+1}{7} \times \frac{6-5}{6}\right] \times 10 = 53{,}8$$

from table 1, I determine that these working conditions belong to the fifth category of labor severity, which means that the worker develops a fairly stable pathological condition, which is characterized by a slowdown in reactions;

b) after taking measures to improve working conditions.

Since after the events the time of exposure to factors of the working environment and working conditions has changed, it is necessary to recalculate the assessment of factors.

We take the shift duration equal to 480 minutes.

In our case, after the events, the time of exposure to noise changed (an excess of the noise remote control was recorded), so a point assessment must be carried out taking into account this change:

$$X_{kop\ 1} = 3 \times \frac{420}{480} = 2{,}625\,,$$

and when changing the duration of neuro-emotional stress:

$$X_{kop\ 2} = 1 \times \frac{240}{480} = 0{,}5.$$

The integral point score after the event taking into account the correction will be equal to:

$$U_2 = \left[3 + \frac{1 + 2{,}625 + 1 + 1 + 2 + 1 + 0{,}5}{7} \times \frac{6-3}{6}\right] \times 10 = 36{,}5\,,$$

from table 1 I determine that these working conditions belong to the third category of labor severity. Under such conditions, reactions occur that are characteristic of the initial stage of the boundary state of the organism.

Forecast for changes in injuries resulting from a better measure of improvement We perform as follows. The growth of injuries for the risk of injury is estimated by formula (5.3).

Let us determine the growth of injuries prior to measures to improve working conditions:

$$Y_1 = \frac{1}{1{,}3 - 0{,}0185 \times 53{,}8} = 3{,}28\ .$$

After the event (changing the air temperature of the working environment, reducing the noise level and time of exposure to the operator, etc.), the category of labor severity will decrease to the third (U2 = 38.3), which will correspond to an increase in injuries of 1.69 times compared to with rational working conditions:

$$Y_2 = \frac{1}{1{,}3 - 0{,}0185 \times 36{,}5} = 1{,}6\ .$$

In carrying out measures to improve working conditions, the severity category changed from fifth to third. As noted above, the severity of labor negatively affects the degree of fatigue, and hence the ability of a person to work. To study the dynamics of changes in health and productivity, it is necessary to calculate the values of indicators of fatigue and health:

a) before the complex of events:

- fatigue indicator by the formula (5.3):

$$Y_1 = \frac{53{,}8 - 15{,}6}{0{,}64} = 60;$$

- the level of performance by the formula (5.4):
-

$$R_1 = 100 - 60\ ;$$

b) after a set of measures:
- fatigue indicator:
-

$$Y_2 = \frac{36{,}5 - 15{,}6}{0{,}64} = 33;$$

- level of performance:

$$R_2 = 100 - 33\ .$$

Change in labor productivity (increase in labor productivity) due to changes in working capacity according to formula (5.5) will be:

$$\Pi_{nm} = \left[\frac{R_2}{R_1} - 1\right] \times 100 \times 0{,}2 = \left[\frac{67}{40} - 1\right] \times 100 \times 0{,}2 = 13{,}5\ .$$

5.2 Calculation of the number and type of fire extinguishers

Geometrical dimensions of the warehouse: - width 72 m; length 96 m; room height to the floor or to the bottom of the beam structures (floor) - 13.5 m; Warehouse area: 5,265.3 m2; The building is one-story; Functional fire hazard F5.2; Fire hazard category B-1.

There are several sections in the warehouse that are not separated by fire barriers with a fire resistance of at least EI45.

Technological map of the room is shown is shown in Figure [5.1].

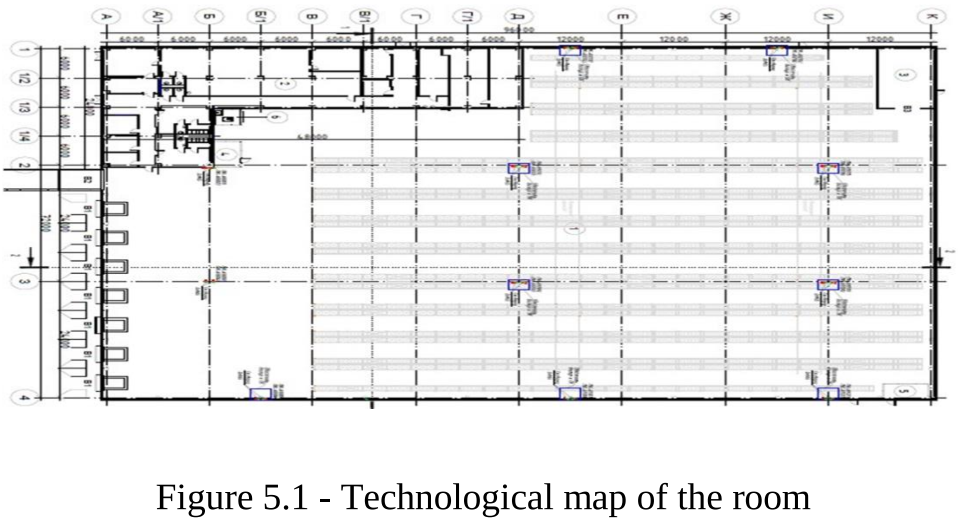

Figure 5.1 - Technological map of the room

The object of operation: ABCh - administrative part - office of OOO “OOO”.

The geometric dimensions of the ABCh: - width 12 m; length 48 m; the height of the room to the floor or to the bottom of the beam structures (floor) - 3.5 m; Floor area: 5,265.3 m2; The building is one-story; Functional fire hazard F4.

Floor plan is shown in Figure 5.2.

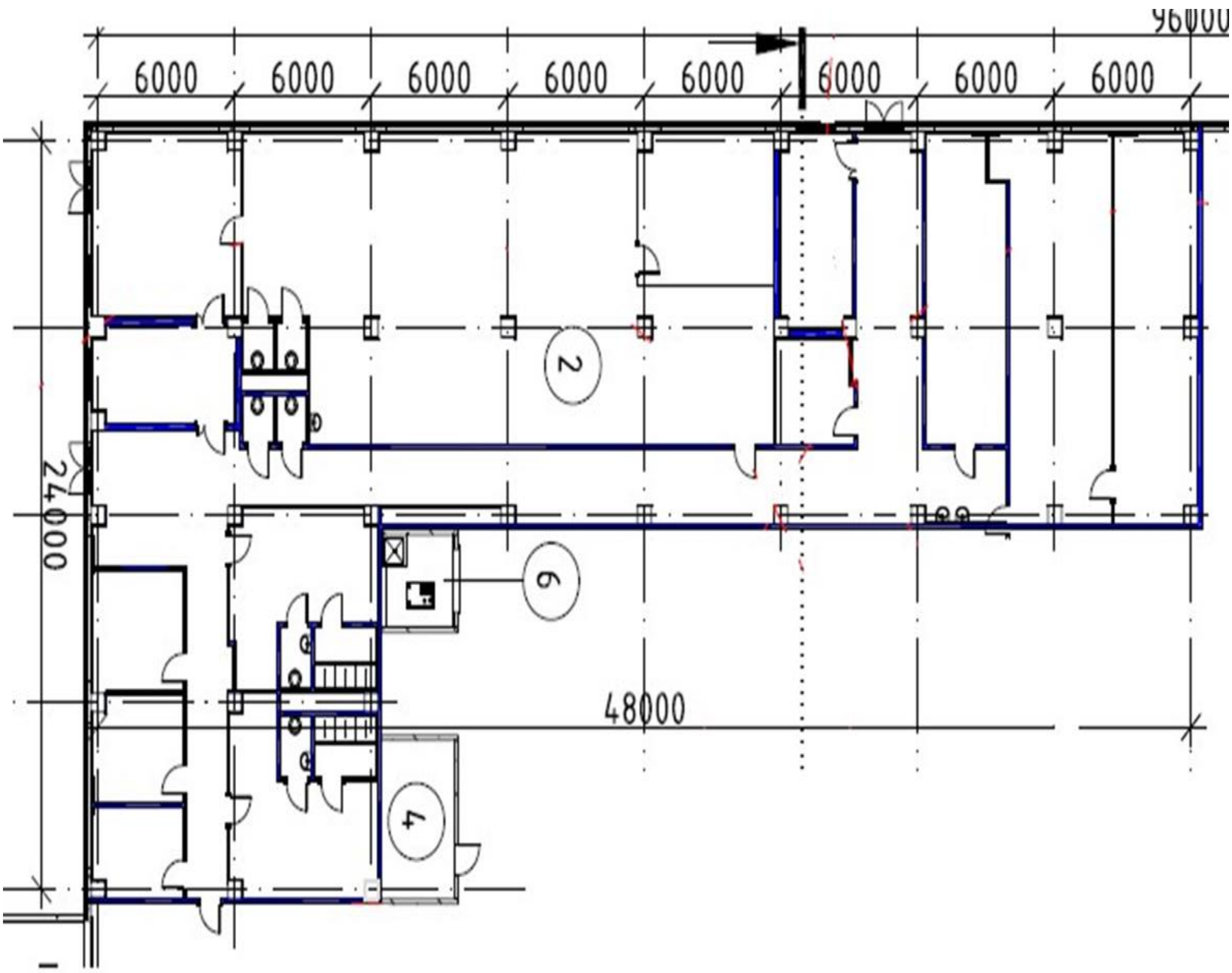

Figure 5.2 - Floor plan

Table 5.4 - Calculation table

№	Name of the building, premises	Area m2	Functional fire hazard	Fire hazard category	Fire class	A type fire extinguisher	Weight OTV fire-shitel, kg	Number of fire flaps
1	Shelf storage area	5000/2500	Ф5.2	B-1	A	Powder mobile	ОП-100 or ОП-50	6 or 11

Continued table 5.4

2	Goods acceptance and shipment area	360/180	Ф5.2	В-1	А	Hand Powder	ОП-10(з) or ОП-6(з)	7 or 14
3	Directory Plot	160/80						
4	Traction charging room rechargeable batteries	100	Ф5.1	В-4	А, Е	Hand Powder	ОП-5	1
						coal acid manual	ОУ-3	1
						ПП-600	1,5x2,0	1
						fire shield	ЩП-Е	1
5	Forklift truck with traction battery	1			А, Е	Hand Powder	ОП-2(з)	1
6	Office	650	Ф4.3		А	Hand Powder	ОП-4(з)	12

Fire extinguisher type identification :

1. Warehouse (shelf storage zone, goods reception and shipment zone, goods shipment zone, catalog area) with a total area of 5 150 m^2. The height of the stacks (fuel load) 2 meters. The height of the shelves is 12 m. To protect the warehouse from fires, taking into account fire class “A”, fire hazard category “B-1”, the height of the combustible load is 12.5 meters, the presence of automatic fire extinguishing systems, primary fire extinguishing systems are combined from OP powder mobile fire extinguishers -100 rank of extinguishing the model hearth 10A and powder manual fire extinguishers weighing ОП-10 (h) with the rank of extinguishing the model hearth 4A;

2. Charging room for traction batteries with an area of 100 m^2.. To protect the premises from fires, taking into account fire class “A” “E”, a height of a combustible load of 2.0 meters, the presence of automatic fire extinguishing systems, primary fire extinguishing systems is provided by an ОП-4 powder fire extinguisher with a fire extinguishing rank of model hearth 2A and carbon dioxide OU-3 , a fire-prevention cloth in the size 1,5x2,0, a fire shield of a complete set "E";

3. Forklift trucks are equipped with portable powder fire extinguishers OP-2 (h) GOST 16215-80, clause 2.1.16 POT RM-008-99);

4. To protect office (administrative and domestic) premises from fires, taking into account their electrification, fire class, primary fire extinguishing agents, portable powder fire extinguishers ОП-4 (h) are used.

5. Server To protect the server rooms, taking into account the specifics of the interaction of fire extinguishing agents with the protected equipment, products and materials, they are used chladone or carbon dioxide fire extinguishers. (Clause 4.7.2. as amended by Decree of the Government of the Russian Federation of February 17, 2014 N 113).

Calculation of the number of primary fire extinguishing agents

The number of primary fire extinguishing agents depends on:

1) from the maximum area to be protected by one fire extinguisher or a group of fire extinguishers;

2) from the maximum distance from a possible fire source to the nearest fire extinguisher, for rooms with a fire hazard category B - must not exceed 30 m;

3) from the placement of technological equipment in the premises. Bulky technological equipment reduces the maximum permissible distance from a fire extinguisher to a possible source of fire;

4) from the location of walls and partitions, as well as the geometry of the room;

5) from the presence or absence of fire extinguishing systems;

6) for economic reasons, for example, in rooms with a large area, it is necessary to install fire extinguishers with a larger capacity.

Considering that the various zones in the warehouse (the shelf storage zone, the goods reception and shipment zone, the goods shipment zone, the catalog section) are not separated by fire barriers, they have one fire load, one fire hazard category, one fire class and one physical and chemical and fire hazardous properties of flammable substances, then, on the basis of clause 47 of the Russian Federation's PPR, the number of fire extinguishers is determined for a single space.

To protect against fire a space with a combustible load of up to 4.5 meters, the calculation of the required number of hand-held fire extinguishers is carried out in accordance with Appendix No. 1 of the RF fire extinguisher from the calculation of the protected area for the placement of a combustible load of 400 m^2. with a K-fire extinguisher (Section 465 of the RF fire extinguisher).

A) Determine the approximate number of fire extinguishers, depending on the maximum coverage area of one K-extinguisher:

$$N_{оп1} = Sп : So \tag{5.8}$$

Where, : Nop1 - the approximate number of fire extinguishers

K - the number of fire extinguishers in one zone - 1 ОП-10 (2 OP-6)

Sp - area of the combustible load of the room: 4900 + 100 + 50 = 5050 m2 So maximum area to be protected by one fire extinguisher - protection zone.

So = 400 m^2. (p. 465, Appendix No. 2 of the RF PPR)

$$N_{оп1} = Sп : So \; N_{оп1} = 5\,150 : 400 = 12{,}875$$

Requires 13 protection zones with hand-held fire extinguishers. Hence the number of fire extinguishers is 13 • K = 13 ОП-10 or 26 ОП-6.

B) We determine the approximate number of hand-held fire extinguishers depending on the maximum distance from the fire extinguisher to a possible source of fire.

$$N_{оп2} = (a : 30) \bullet (b : 30) \bullet K^2 \tag{5.9}$$

Where, Nop2 - the approximate number of fire extinguishers;

K - the number of fire extinguishers per zone - 2 ОП-6; a - room depth 96 m; b - the width of the room, 72 m;

30 - the maximum distance from a possible fire source to the location of the fire extinguisher;

$$N_{оп2} = (a : 30) \bullet (b : 30) \bullet 2K \tag{5.10}$$

$$N_{оп2} = ((96\text{-}6) : 30) \bullet ((72\text{-}6) : 30) \bullet 2K = 13{,}2$$

Requires 14 protection zones with hand-held fire extinguishers. Hence the number of fire extinguishers is 14 • K = 14 ОП-10 or 28 ОП-6.

As a result, to protect the warehouse, we accept the number of fire extinguishers:7 pcs ОП-10 or 14 pcs. ОП-6;

6 Feasibility study of the project

Business plan

In this chapter, I conduct detailed calculations that I make and study the device, that is, the flexible manipulator – the economic component of the business plan. To do this, first, I will give a brief overview of the business plan as a whole.

A business plan is a document that sets out the economic goals of an enterprise or entrepreneur and the ways to implement it, its tasks and methods. To create a business, the market environment is thoroughly studied. The current state of the market environment, possible changes and barriers, the amount of revenue from the project, and so on. A business plan is primarily designed to obtain a loan from a Bank and ensure its repayment. With the participation of the owner, the direction of strategic development of the enterprise is determined, thereby determining the effectiveness and necessity of the project.

In the business plan I created, I plan to make a summary, description, product marketing, financial plan, calculation of investment costs, cost and economic efficiency.

Summary

The calculation of the economic efficiency of absolutely any project is an integral part of the development of the project, because it makes no sense to implement unprofitable development in advance. The costs of implementing any software tool depend on material costs for resources, developer wages, including social security contributions, depreciation expenses, and others. The technical equipment obtained as a result of the development of the graduation project is two-legged robot

1) The complexity of developing a software project

The main tasks of work planning are:

– determination of the scope of upcoming work;

– mutual coordination of work and the establishment of a rational sequence of upcoming work;

– establishment of work.

– Planning work is reduced to compiling a list of works, determining their complexity, calculating the duration of the work cycle, substantiating the cost estimates for the work.

Table 6.1 -

SP Development Stages	Types of jobs	The complexity of development, people× h
1 stage	Domain Analysis	6
2 stage	Formulation of the problem	2
3 stage	Development of technical specifications	8

Continued table 6.1

4 stage	Project assembly	8
5 stage	Equipment testing	12
TOTAL software product		36

2) Calculation of development costs SP

To determine the costs of developing SP, you need to make an estimate, which includes the following articles:

-material costs;

- costs to pay for the trade;

-social tax ;

-amortization of fixed assets;

-other expenses;

Material costs

The costs of basic auxiliary materials relate to material costs. Calculation of the cost of material resources and the cost of equipment are made in the form given in 5.2 - 5.3

Table 6.2 - the cost of hardware and software

№	Name	Description	Price per unit, tg	The amount, tg
1	A laptop	Lenovo	150 000	150 000
2	operating system	Microsoft Windows 10	free	free
3	Matlab		7000	7000
4	TP-LINK Wi-Fi Router	1	6000	6000
5	SG90 9G servotec	1	900	900
6	Bluetooth module HC-06 from the adapter panel	1	1500	1500
7	SMC directional valves SY3260- 5LOU-C6- Q	1	3000	3000
8	Welding station	1	5000	5000
9	Power Supply 12V-1A		4200	4200
10	Additional expenditure			9300
TOTAL hardware and software costs				186900

Table 6.3 - the Cost of material resources

	Name	Description	Price per unit, tg	The amount, tg
	Paper	A4	1 000	1 000
TOTAL hardware and software costs				1 000

Electricity Costs

This chapter includes technological costs, which are provided in table 5.4. The total cost is calculated by the formula (6.1).

$$T_c = \sum_{i=1}^{n} M_i * K_i * T_i * C \qquad (6.1)$$

From January 1, 2019, the electricity price at the tariff of «AlmatyEnergoSbyt!» is 15.90 tg per 1 kWh, excluding Value added tax. The price of electricity, including Value added tax, will be 17.81 tg per 1 kWh.

Table 6.4 - Costs for technological needs

Name of equipment	Nameplate power kWh	Power factor	Development equipment uptime h	The price of electricity tg/ kWh	The amount, tg
A laptop	0.2	0.8	157	17.81	447.387
Total electricity costs					447.387

Labor costs

Labor costs are calculated according to the form given in table 5.5. The total cost of labor is calculated according to the formula (6.2)

$$L_c = \sum_{i=1}^{n} C_i * T_i \qquad (6.2)$$

The hourly rate of the employee, calculated by the formula, is - 400 tg/hour.

The monthly salary of a beginning electronic engineer who participated in the development of this project = 60000 tg

Table 6.5 – the Cost of labor

Employee category	The complexity of development,h	Hourly rate, tg/h	The amount, tg
Developer	1x150	400	60 000
Total cost of labor			60 000

Social tax

Social security contributions account for 9.5% of salaries for the wages of all employees, however, pension contributions (10% of Зтр) are not subject to social tax.

Mandatory pension contributions will amount to 60000*10%=6000 tg

From here, the amount of social tax will be (60000-6000)*9.5%=5 130 tg

Depreciation of fixed assets

Under the article "Depreciation of fixed assets" are calculated depreciation charges, based on the value of fixed assets, used in the process of developing a software product, terms equipment operation and annual depreciation rates. Depreciation deductions are determined in accordance with Table 5.6. The amount of depreciation is calculated by the formula (6.3).

$$D_d=\frac{Ic*N\text{a}*N}{100*12*t} \tag{6.3}$$

Where, N_a- depreciation rate (%);

I_c- initial cost of equipment;

N- equipment usage time;

t- number of working days in a month.

$$D_d =(150000*0,125*25)/(1*12*24)=1627.6 \text{ tg.}$$

$$D_d =(7000*0,125*25)/(1*12*24)=75.95 \text{ tg.}$$

$$D_d =(6000*0,125*25)/(1*12*24)=65.104 \text{ tg.}$$

$$D_d =(900*0,125*25)/(1*12*24)=9.76 \text{ tg.}$$

$$D_d =(1500*0,125*25)/(1*12*24)=16.276 \text{ tg.}$$

$$D_d =(3000*0,125*25)/(1*12*24)=32.55 \text{ tg.}$$

$$D_d =(5000*0,125*25)/(1*12*24)=54.253 \text{ tg.}$$

$$D_d =(4200*0,125*25)/(1*12*24)=45.57 \text{ tg.}$$

$$D_d =(9300*0,125*25)/(1*12*24)=100.911 \text{ tg.}$$

Table 6.6- Depreciation of fixed assets

Name of hardware and software	The cost of hardware and software, tg	Annual depreciation rate, %	Development time of equipment and software for development ПП, д	The amount, tg

table continuation 6.6

A laptop	150 000	12.5	25	1627.6
Matlab	7000	12.5	25	75.95
TP-LINK Wi-Fi Router	6000	12.5	25	65.104
SG90 9G servotec	900	12.5	25	9.76
Bluetooth module HC-06 from the adapter panel	1500	12.5	25	16.276
Power Supply 12V-1A	4200	12.5	25	45.57
Welding station	5000	12.5	25	54.253
SMC directional valves SY3260- 5LOU-C6- Q	3000	12.5	25	32.55
Additional expenditure	9300	12.5	25	100.911
TOTAL depreciation of fixed assets				2027.974

Table 6.7 - the cost of other expenses

Name	quantity	time	price, tg	The amount,tg
the Internet	-	2 months	4000	8000
advertising	-	1 mon	12000	12000
Total expenses for other expenses				20000

When developing the equipment, Internet resources were used, the costs of which amounted to 8,000 tg per month. Also, the payment for advertising amounted to 12,000 tg. Total for other expenses, the amount is 20,000 tg.

Cost estimate for the development of software

Having calculated the costs associated with the creation of a robot, based on the calculations obtained in paragraphs 4-8, a cost estimate was made and reflected in table 6.8

Table 6.8 - Estimated development costs SP

Cost item	amount, tg
Salary	60000
Social tax	5130
Electric power	447.387
Depreciation of fixed assets	2027.974
Other expenses	20000
Total estimate	87605.361

Determination of the possible (contractual) SP

The value of the possible (contractual) price of software is established on the basis of efficiency, quality and terms of its implementation at a level that meets the economic interests of the customer (consumer) and contractor and is calculated by the formula (6.5).

$$C_d=З_{нир}(1+\frac{P}{100}) \qquad (6.5)$$

P– the average level of profitability of SP is taken at a rate of 20%

$$C_d=87605.361*(1+0,2)= 105126,433 \text{ tg.}$$

Then the sales price is determined, including value added tax (VAT), and the rate (VAT) is set by law. The tax Code of the Republic of Kazakhstan for 2020 sets the VAT rate at 8% starting from March.

The selling price including VAT is calculated according to the formula (5.6):

$$C_p=C_d+ C_d*VAT \qquad (5.6)$$

$C_{p=}$105126,433 +105126,433*0.08=113 536,5 (tenge)

The calculated possible price of SP is 113 536,5 tg.

Conclusion

The goal of this thesis was to develop systematic approach for dynamic modeling and control of spatial flexible manipulators. The thesis work on flexible manipulators was divided into two parts. The first part was focused on dynamic modelling of spatial flexible manipulators while the second part was focused on control design of spatial flexible manipulators for trajectory tracking.

A general purpose multi-body code has been developed to obtain a nonlinear dynamic model of spatial flexible manipulators for model based control design and simulation purposes. Both link and joint flexibilities can be included in the dynamic modeling. The flexible links are discretized to get a finite dimensional dynamic model.

The deformation of each link is assumed to be due to both bending and torsion. The deformation of the joints is assumed to be due to pure torsion. The deformation of each link is assumed to be small relative to the rigid body motion. Thus, the configuration of each link is defined as the sum of rigid and elastic coordinates using a floating reference frame. The dynamic model is first derived using the principle of virtual work along with finite element method in generalized coordinates for general purpose implementation. Then, the system of equations in generalized coordinates is converted into independent coordinate form using a recursive kinematic formulation based on the topology of a manipulator.

The advantage of general purpose multi-body code is that it uses minimum set of equations that define the dynamics of flexible manipulator, which is required in control design to reduce computation cost. In addition, it allows the dynamic modeling of any arbitrary manipulator configuration that consists of rigid links, flexible links and flexible joints.

Numerical simulation results of an open chain RRR spatial manipulator with flexible links and flexible joints was presented to show the effects of flexibility on robot manip ulator dynamics. The simulations results showed that the link and joint flexibility can alter the motion of endeffector in workspace. Thus, Ignoring the link or joint flexibility can cause poor estimation of dynamic parameters and, eventually, poor performance of the control design.

Model based controllers were developed for trajectory tracking and vibration suppression of spatial flexible link manipulators. The following model based controllers were designed for an open chain RRR spatial flexible link manipulator:

- PD Control
- Stable Inversion Control
- A Nonlinear Control
- Adaptive Control

Among them, PD control and Stable inversion control are derived using feedback linearization technique. A nonlinear control and Adaptive control are derived using sliding mode technique.

The simulation results of PD controller showed good trajectory tracking at joint space. However, it is not very efficient to damp the endeffector vibrations. The stable inversion control showed better trajectory tracking compared to PD control, however this method is incapable of damping the vibrations in case of unmodeled dynamics such as unknown payload mass. Moreover, stable inversion control can have good performance for planar flexible link manipulators compared to spatial flexible link manipulators.

Nonlinear controller and adaptive controller showed good trajectory tracking at the joint space and also efficient to damping the endeffector vibrations compared to PD controller and stable inversion controller.

Experimental results on a single link flexible manipulator showed that the adaptive controller has better trajectory tracking and vibration suppression compared to PD control and stable inversion control in the presence of additional unknown payload mass on the endeffector.

Through the present work, the state of the art developed for planar flexible links manipulators was extended to a spatial flexible link manipulators. It is learnt that the spatial flexible link manipulators require additional control effort to damp the out of plane vibration modes. These vibration modes are due to out of plane bending effect. The future work on spatial flexible link manipulators can be focused to improve the damping properties of out-of-plane vibration modes. Further studies can be focused on the additional actuator and its positions to damp the out-of-plane bending modes.

Bibliography

1 A. Akira, and K. Komuro. An energy saving open-loop control technique for flexible manipulators. *International Conference on Mechatronics and Automation*, pages 416–421, 2011.

2 A. Albu-Schaffer, O. Eiberger, M. Grebenstein, S. Haddadin, C. Ott, T. Wimbock, S. Wolf, and G. Hirzinger. Soft robotics: From torque feedback controlled lightweight robots to intrinsically compliant systems. *IEEE Robotics and Automation Mag.*, 15(3):20–30, 2008.

3 A. Daryabor, A.H. Abolmasoumi, and H. Momeni. . Robust pole placement control of flexible manipulator arm via lmis. *41st Southeastern Symposium on System Theory*, pages 274–279, 2009.

4 A. De Luca, B. Siciliano. Closed-form dynamic model of planar multi-link lightweight robots. *IEEE Transactions on Systems, Man, and Cybernetics*, 21(4):826–839, 1991.

5 A. De Luca, S. Iannitti, R. Mattone and G. Oriolo. Control problems in underactuated manipulators. *IEEE/ASME International Conference on Advanced Intelligent Mechatronics*, 2:855–861, 2001.

6 A. Konno, L. Deman, and M. Uchiyama. A singularly perturbed method for pole assignment control of a flexible manipulator. *Robotica*, 20(6):637–651, 2002.

7 A. Shabana. *Dynamics of Multibody Systems*. Cambridge University Press, 2005.

8 A.De. Luca. Trajectory control of flexible manipulators. *Control Problems in Robotics and Automation*, pages 83–104, 1998.

9 A.De. Luca, and B. Siciliano. Joint-based control of a nonlinear model of a flexible arm. *Proceedings of IEEE in American Control Conference*, pages 935–940, 1988.

10 A.De. Luca and B. Siciliano. Trajectory control of a non-linear one-link flexible arm. *International Journal of Control*, 50(5):1699–1715, 1989.

11 A.De. Luca, and B. Siciliano. Inversion-based nonlinear control of robot arms with flexible links. *Journal of guidance, control, and dynamics*, 16(6):1169–1176, 1993.

12 A.De. Luca, F. Nicolo, and G. Ulivi. Trajectory tracking in flexible robot arms. *System Models and Feedback: Theory and Applications*, pages 17–34, 1992.

13 A.De. Luca, S. Panzieri, and G. Ulivi. Stable inversion control for flexible link manipulators. *IEEE International Conference on Robotics and Automation*, 1:799–805, 1998.

14 A.H. Abolmaasoumi, H.R. Momeni, and A. Daryabor. Robust Î¼-synthesis control of a flexible manipulator arm. *41st Southeastern Symposium on System Theory*, pages 330–334, 2009.

15 Atsushi Konno and Masaru Uchiyama. Modeling of a flexible manipulator dynamics based on the holzers method. *IEEE/RSJ International Conference on Intelligent Robots and Systems*, 1:223–229, 1996.